

Ultra-low-noise transimpedance amplifier with a single HEMT in pre-amplifier for measuring shot noise in cryogenic STM

Ying-Xin Liang^{1,2*},

¹Beijing Academy of Quantum Information Sciences,
No.10 Xibeiwang East Road, beijing, 100193China

²Coll Phys & Elect Engn, Anyang Normal University,
No.436, Xiang Avenue, Anyang 455000, Henan, China

December 3, 2023

Abstract

In this work, a design of transimpedance amplifier (TIA) for cryogenic scanning tunneling microscope (CryoSTM) is proposed. TIA with the tip-sample component in CryoSTM is called as CryoSTM-TIA. With transimpedance gain of $1\text{ G}\Omega$, the bandwidth of the CryoSTM-TIA is larger than 300 kHz . The distinctive feature of the proposed CryoSTM-TIA is that its pre-amplifier is made of a single cryogenic high electron mobility transistor (HEMT), so the apparatus equivalent input noise current power spectral density at 100 kHz is lower than $4\text{ (fA)}^2/\text{Hz}$. In addition, “bias-cooling method” can be used to in-situ control the density of the frozen DX^- centers in the HEMT doping area, changing its structure to reduce the device noises. With this apparatus, fast scanning tunneling spectra measurements with high-energy-resolution are capable to be performed. And, it is capable to measure scanning tunneling shot noise spectra (STSNS) at the atomic scale for various quantum systems, even if the shot noise is very low. It provides a powerful tool to investigate novel quantum states by measuring STSNS, such as detecting the existence of Majorana bound states in the topological quantum systems.

1 Introduction

High performance transimpedance amplifier (TIA) for cryogenic scanning tunneling microscope (CryoSTM) is a key element [1, 2]. Recently, in Ref.[3], it was proposed a design of TIA for CryoSTM. TIA with the tip-sample component in CryoSTM is called as CryoSTM-TIA. In that design, the CryoSTM-TIA has a transimpedance gain of $1\text{ G}\Omega$, a bandwidth of more than 300 kHz , and its equivalent input noise current power spectral density (PSD) that characterizes the circuit inherent noise is $21\text{ (fA)}^2/\text{Hz}$ at 100 kHz . The CryoSTM-TIA is capable of measuring the scanning tunneling shot noise spectra (STSNS) of various quantum systems at atomic resolution, even if the measured noise

*cryoliang@qq.com

current PSD is as small as a few $(\text{fA})^2/\text{Hz}$. In Ref.[3], it was illustrated how the CryoSTM-TIA is used to measure STSNS of quantum systems to investigate novel quantum states, such as detecting Majorana bound states (MBSs) in iron-based superconductors [4]. In the CryoSTM-TIA, cascade the pre-amplifier (Pre-Amp) and the post-amplifier (Post-Amp) to form an operational amplifier (OPA), and denoted as Macro-OPA. Pre-Amp in Macro-Amp is a differential amplifier made of a pair of high electron mobility transistors (HEMTs), where the HEMT is a kind of cryogenic GaAs MESFET [5, 6]. However, it is quite difficult to select cryogenic GaAs MESFETs with identical performances for pairing [2].

In this work, a design for the CryoSTM-TIA with a single HEMT in Pre-Amp is proposed. In the CryoSTM-TIA, cascade Pre-Amp and Post-Amp to form an inverting-amplifier (Inv-Amp), which is not OPA. The CryoSTM-TIA still has transimpedance gain of $1\text{G}\Omega$ and bandwidth more than 300 kHz. However, its equivalent input noise current PSD is only $3 (\text{fA})^2/\text{Hz}$ at 100 kHz, i.e. $1/7$ of that in Ref.[3], since a noisy HEMT is reduced. Therefore, the lower tunneling shot noise of quantum systems can be measured at the atomic scale with this apparatus. Furthermore, only a single HEMT is used in Pre-Amp, avoiding the difficulty of matching two identical HEMTs. And, “bias-cooling method” [5] can be used to in-situ reduce the inherent noise of the HEMT. With these advantages, this apparatus will be a powerful tool to investigate novel quantum states in various quantum systems, in the wider range of applications than that in Ref.[3], such as high- T_c superconductors [7, 8], topological superconductors [4], MBSs [4, 9, 10, 11, 12], Andreev reflection [13, 14], and Kondo effect [15], etc.

2 Circuit of the proposed CryoSTM-TIA

The circuit of the proposed CryoSTM-TIA is shown in Fig.1. It consists of several components: the single HEMT amplifier part of Pre-Amp shown in dashed box (a1) of Fig.1, the constant-current source part of Pre-Amp in dashed box (a2), the post-amplifier (Post-Amp) shown in dashed box (b), the compensated feedback network shown in dashed box (c), and the signal source circuit shown in dashed box (d). The two stage amplifier made of Pre-Amp and Post-Amp is called as inverting-amplifier (Inv-Amp). Inv-Amp is connected with the feedback network to form TIA. The input G of TIA is connected to the signal source circuit, to form the CryoSTM-TIA. The components placed in the cryogenic zone are shown in the dotted box. The parameters of all components of the CryoSTM-TIA circuit are listed in Table 1.

2.1 Design of Pre-Amp

As shown in Fig.1, only a single cryogenic HEMT is used in Pre-Amp. The HEMT in this work is CNRS-HEMT (denoted as C-H) [5, 6] developed by CNRS/LPN in France with the excellent cryogenic and noise characteristics. It is capable of operating under 0.5 K with only 0.1 mW on the ideal operating point of “ $V_{ds} = 100 \text{ mV}$ and $I_{ds} = 1 \text{ mA}$ ”. Its parameters are listed in Table 1, where e_H^2 is its equivalent input noise voltage PSD and i_H^2 is its equivalent input noise current PSD [6].

The single HEMT amplifier part of Pre-Amp is shown in dashed box (a1) in Fig.1. The source of C-H is grounded by a resistor R_s and a small variable resistor R_{s1} . $R_S = R_s + R_{s1}$,

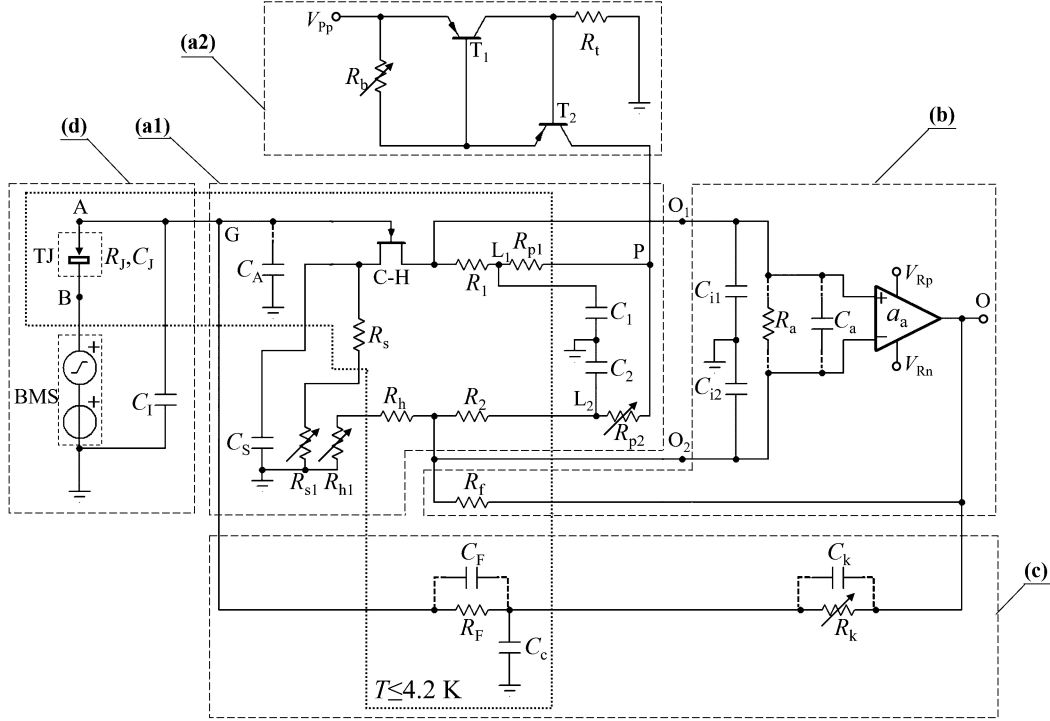


Figure 1: Circuit of the proposed CryoSTM-TIA. Single HEMT amplifier part of Pre-Amp is shown in dashed box (a1), constant-current source part of Pre-Amp in dashed box (a2), Post-Amp in dashed box (b), compensated feedback network in dashed box (c), and signal source circuit in dashed box (d). The components placed in the cryogenic zone are shown in the dotted box. The parameters of all components of CryoSTM-TIA circuit are listed in Table 1.

and a capacitor C_S of 0.1 mF is in parallel with R_S . Drain O_1 of C-H is connected to the load resistor R_1 , and L_1 as the other end of R_1 is connected to output P of the constant-current source through a small resistor R_{p1} . The resistor R_h is grounded through the variable resistor R_{h1} . $R_H = R_h + R_{h1}$. The other end of R_h , denoted as O_2 , is connected to the resistors R_2 , and L_2 as the other end of R_2 is connected to P through a small variable resistor R_{p2} . $R_1 = R_2 = R_L$. L_1 and L_2 are grounded by the capacitors C_1 and C_2 respectively, and $C_1 = C_2 = C_L = 10 \mu\text{F}$. C_A is the input capacitance of Pre-Amp. C-H, R_s , R_h , R_1 , R_2 , and R_{p1} are placed in the cryogenic zone, shown in the dotted box. C_1 is the capacitance of the cable that connects gate G of C-H and the tip in the CryoSTM. C-H is as close to the tip as possible to reduce C_1 , which can be less than 0.5 pF [18]. The operating point adjustment for Pre-Amp is shown in Sect.4. The Pre-Amp parameters are shown in Table 1.

For Pre-Amp, when AC voltage \dot{V} is applied to input G, the AC voltage difference between O_1 and O_2 is denoted as \dot{V}_{op} . $A_{vP} = \dot{V}_{op}/\dot{V}$ is the voltage gain of Pre-Amp. Since the gain-bandwidth-product of the CNRS-HEMT is $g_m/[2\pi(C_{gs}+C_{gd})] \approx 1 \text{ GHz}$, the bandwidth of Pre-Amp is more than 30 MHz. In $\max\{g_m/(2\pi C_S), 1/(2\pi R_S C_S), 1/(2\pi R_S C_2)\} \ll$

Table 1: Parameters of all components of CryoSTM-TIA circuit

CNRS-HEMTs C-H			
Gate-source resistance R_A		$>10 \text{ T}\Omega$	
Transconductance g_m		40 mS	
Channel conductance g_d		1 mS	
Gate-source capacitance C_{gs}		5 pF	
Gate-drain capacitance C_{gd}		1 pF	
Drain-source voltage V_{ds}		100 mV	
Drain-source current I_{ds}		1 mA	
$e_H^2 \text{ ((nV)}^2/\text{Hz})$	10 kHz	0.25	
	100 kHz	0.07	
$i_H^2 \text{ ((fA)}^2/\text{Hz})$	10 kHz	0.1	
	100 kHz	1	
Pre-Amp			
R_S	$100 \pm 5 \text{ }\Omega$	C_S	0.1 mF
R_H	$200 \pm 5 \text{ }\Omega$	R_L	1 k Ω
R_{p1}	10 Ω	R_{p2}	$10 \pm 10 \text{ }\Omega$
C_1 & C_2	10 μ F		
T_1 & T_2	BJT BFT93 [16]	R_b	$347 \pm 1 \text{ }\Omega$
R_t	20 k Ω	V_{Pp}	+12 V
Post-Amp with THS4021 as Rear-OPA			
a_{a0}	97.5 dB	f_b	14.5 kHz
C_a	1.5 pF	R_a	1 M Ω
R_f	330 k Ω	C_i	100 pF
Supply voltages V_{Rp}, V_{Rn}		+15, -15 V	
Feedback network			
R_F	1 G Ω	C_F	$\sim 0.3 \text{ pF}$
R_k	100 k Ω	C_k	$\sim 0.2 \text{ pF}$
C_c	3 nF		
Signal source circuit			
R_J	$\geq 1 \text{ M}\Omega$	C_1	$\sim 0.5 \text{ pF}$

Note: \pm indicates the variable resistance range. Without specification, the default value after \pm is 0.

$f \leq 3 \text{ MHz}$ (i.e. $112 \text{ Hz} \ll f \leq 3 \text{ MHz}$ with the parameters listed in Table 1),

$$A_{vP} \approx -g_m R_d, \quad (2.1)$$

where $R_d = R_L/(1 + R_L g_d)$. i.e., $A_{vP} \approx -20$ in $112 \text{ Hz} \ll f \leq 3 \text{ MHz}$. The input capacitance of Pre-Amp is

$$C_A = C_{gs} + (1 - A_{vP})C_{gd}. \quad (2.2)$$

i.e., $C_A \approx 26 \text{ pF}$ in $112 \text{ Hz} \ll f \leq 3 \text{ MHz}$. The input resistance of Pre-Amp R_A is the gate-source resistance of C-H, and $R_A > 10 \text{ T}\Omega$, so it can be considered as infinity.

The constant-current source part of Pre-Amp shown in the dashed box (a2) in Fig.1 is the same as in Ref.[3]. For a given resistance R_b , there is almost no fluctuation for the current I_{sour} generated by the constant-current source, even though the voltage V_{Pp} of the positive voltage source fluctuates greatly, which ensures the stability of the operating point for C-H.

2.2 Design of Post-Amp and composition of Inv-Amp

In Fig.1, the Post-Amp circuit in the dashed box (b) is the same in structure as that in Ref.[3]. There is a commercial operational amplifier (OPA) in the circuit, called as Rear-OPA, which is the OPA with high gain-bandwidth-product, such as THS4021, OPA657, and LMH6624, etc. R_a and C_a are the input resistance and capacitance of Rear-OPA respectively. The feedback resistor R_f is connected to output O of Rear-OPA and its inverting input. R_f is 330 k Ω , and it placed in the cryogenic zone. Post-Amp also contains two cables that connect the non-inverting input and inverting input of the Rear-OPA to outputs O₁ and O₂ of Pre-Amp respectively. The capacitance of the two cables is C_{i1} and C_{i2} respectively, and they may vary from 50 pF to 150 pF. In this work, $C_{i1} = C_{i2} = C_i \approx 100$ pF is assumed. The Rear-OPA in this work is THS4021 [17], and $C_i \gg C_a$. The Post-Amp parameters are listed in Table 1.

Cascade Pre-Amp and Post-Amp to form Inv-Amp. For the AC signal, the voltage gain of Inv-Amp is $a_A = a_A(f)$. $a_A(f)$ can be expressed as

$$a_A = A_{vP} A_{vR}. \quad (2.3)$$

By the nodal analysis method, a_A can be obtained. And then, with A_{vP} expressed by Eq.(2.1), A_{vR} can be obtained by Eq.(2.3). In $\max\{g_m/(2\pi C_S), 1/(2\pi R_S C_S), 1/(2\pi R_S C_2)\} \ll f \leq 3$ MHz (i.e. 112 Hz $\ll f \leq 3$ MHz with the parameters listed in Table 1),

$$A_{vR} \approx \frac{R_f}{R_{HL}} \cdot \frac{1 + j2\pi f R_{HL} C_i}{1 + j2\pi f R_d C_i} \cdot \frac{1}{1 + \frac{R_f}{a_a R_{HL}} + j2\pi f \frac{R_f C_i}{a_a}}, \quad (2.4)$$

where $R_{HL} = R_H R_L / (R_H + R_L)$ and a_a is the voltage gain of the Rear-OPA. In this work, $R_f \gg R_{HL}$ and $R_a \gg R_{HL}$. And, a_a can be approximately expressed as $a_a = a_{a0}/(1 + jf/f_b)$ in (0, 40 MHz] for THS4021.

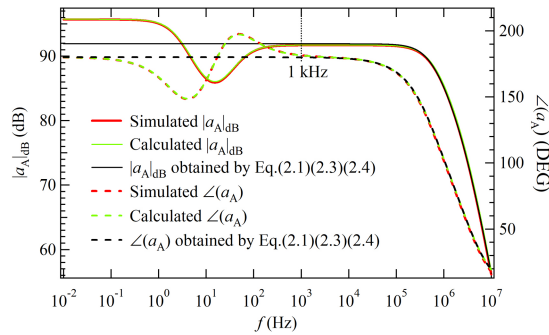


Figure 2: The Inv-Amp voltage gain $a_A(f)$. The solid curves are the curves of $|a_A(f)|_{dB}$, and the dashed curves are the curves of $\angle(a_A(f))$. The red curves are the TINA-TI simulation results, the green curves are the calculated results with the nodal analysis method, and the black curves are the calculated results by Eqs.(2.1), (2.3), and (2.4) in Article.

With the parameters in Table 1, the Inv-Amp performances can be simulated by TINA-TI [19]. Fig.2 show the curves of $|a_A(f)|_{dB}$ and $\angle(a_A(f))$ simulated by TINA-TI. By the

nodal analysis method, $a_A(f)$ is calculated by the equations established with all components listed in Table 1 [20], which is also shown in Fig.2. The curves of $|a_A(f)|_{\text{dB}}$ and $\angle(a_A(f))$ calculated by the nodal analysis method are identical with the simulated ones respectively. $|a_A(f)|_{\text{dB}}$ and $\angle(a_A(f))$ are also calculated by Eqs.(2.1), (2.3), and (2.4), and the calculated curves in Fig.2 are almost identical with the simulated ones respectively in [1 kHz, 10 MHz], which verifies the correctness of Eqs.(2.1),(2.3), and (2.4).

A 1 meter cable with characteristic impedance of 50Ω has a distributed capacitance of 100 pF and a distributed inductance of 250 nH, and its distributed LC structure results in several resonant gain peaks in [80 MHz, 1 GHz] [21]. In Inv-Amp, Post-Amp and Pre-Amp are connected by the cables, and the resonant gain peaks may cause the self-oscillations, as some unexpected electromagnetic couplings may exist among the outputs and the inputs of the amplifiers. The simulations show that, by adding two low-pass filters (with the upper cut-off frequency of 3 to 10 MHz) at the Rear-OPA inputs or at the ends of the cables (depending on the type of low-pass filters being used), these resonant gain peaks can be greatly reduced, thus avoiding the self-excited oscillation.

2.3 Frequency compensation of feedback loop

In order to increase the bandwidth of the CryoSTM-TIA, for the high feedback resistor R_F with parasitic capacitance C_F , frequency compensation must be used in the feedback loop [1, 22]. In Fig.1, the compensated feedback network is shown in the dashed box (c). R_F is placed as near as possible to C-H for reducing the capacitance between the gate G of C-H and Ground. Taking C_c equal to kC_F , where k is above 10^3 , adjust R_k equal to R_F/k , realizing $R_k C_c = R_F C_F$. The output voltage of TIA as \dot{V}_o generates the current \dot{I}_F flowing to input G of TIA, so

$$Z_F(f) = \frac{\dot{V}_o}{\dot{I}_F} \approx \frac{R_k + R_F}{1 + j2\pi f R_k C_k} \approx \frac{R_F}{1 + j2\pi f R_k C_k},$$

where C_k is the parasitic capacitance of R_k [1, 3, 22]. $Z_F(f)$ can be considered as the impedance of the feedback network. In Ref.[22], it has been achieved in experiments to broaden the bandwidth of the feedback network with the very high feedback resistor R_F of 10 G Ω to MHz. In (0, 1 MHz], with the parameters listed in Table 1, $|Z_F(f)| \approx R_F/|1 + j2\pi f R_k C_k| > R_F/1.008$ and $|Z_F(f)| \leq R_F$, so it can be considered that $Z_F(f)$ is equal to R_F .

In order to verify the above frequency compensation method, the following experiment is done. A resistor with 500 M Ω (± 25 ppm/ $^{\circ}\text{C}$) at room temperature is chosen as R_F , which is 1.16 G Ω at 4.2 K. R_k is a 380 k Ω resistor in series with a 0 ~ 20 k Ω potentiometer, and C_c is a COG ceramic capacitor of 10 nF. In order to easily adjust the frequency compensation, a 3 pF capacitor is paralleled with the R_F , so that the C_F is about 3.2 ~ 3.4 pF (estimated as 3.34 pF). Fig.3 shows the experimental results after frequency compensation, in which $|Z_F| = R_F/\sqrt{2}$ at 905 kHz, and φ_{Z_F} as the phase of Z_F is -31.5° at 905 kHz.

2.4 Circuit stability of the proposed CryoSTM-TIA

In Fig.1, the signal source circuit is shown in the dashed box (d), and its parameters are shown in Table 1. The differential resistance of the tip-sample tunnel junction (TJ) is

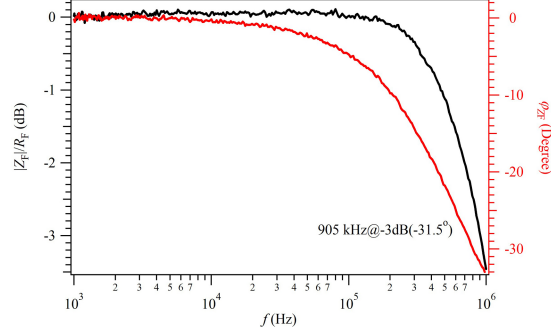


Figure 3: At 4.2 K, R_F is $1.16 \text{ G}\Omega$ and C_F is estimated as 3.36 pF . As $R_k = 390 \text{ k}\Omega$ and $C_c = 10 \text{ nF}$, the black curve shows that the bandwidth of $|Z_F|/R_F$ is broadened to 905 kHz , and the red curve shows φ_{ZF} as the phase of Z_F is -31.5° at 905 kHz .

R_J , which is limited to no less than $10^{-3}R_F$ in this design. The capacitance of TJ is C_J , which is in parallel with R_J . And, C_J is estimated as several fF [3]. $C = C_A + C_I + C_J$ in this work. C_J is at least two orders of magnitude less than $C_A + C_I$, so it can be ignored in C and $C \approx C_A + C_I$. The DC bias & modulated signal voltage source is denoted as BMS, which provides the DC bias V_i and sinusoidal modulated signal voltage \dot{V}_i for the CryoSTM-TIA. In the following simulation, C_I is always taken as 0.5 pF . TIA connects the signal source circuit to form the CryoSTM-TIA. According to the parameters in Table 1, the performances of the CryoSTM-TIA can be simulated by TINA-TI.

The loop gain T_L of the proposed CryoSTM-TIA [23] is

$$T_L(f) = -a_A(f)\beta(f) = -a_A(f)/[1/\beta(f)],$$

in which $\beta(f)$ is the feedback factor, and its reciprocal is,

$$1/\beta(f) \approx 1 + Z_F[1/R_J + 1/R_A + j2\pi f(C_A + C_I)]. \quad (2.5)$$

By Eq.(2.5), $|1/\beta(f)|$ and $\angle(1/\beta(f))$ can be calculated. Fig.4(a) shows the calculated results of $|1/\beta(f)|_{\text{dB}}$ and $\angle(1/\beta(f))$ with $R_J = +\infty$, and Fig.4(b) shows those with $R_J = 1 \text{ M}\Omega$. $|a_A|_{\text{dB}}$ and $\angle(a_A)$ are also shown in Fig.4. Both figures show $|T_L|_{\text{dB}} = |a_A|_{\text{dB}} - |1/\beta(f)|_{\text{dB}} \leq -10 \text{ dB}$ in $f \geq 512 \text{ kHz}$ and $\angle(T_L) = \angle(-a_A) - \angle(1/\beta) = \angle(a_A) - 180^\circ - \angle(1/\beta) > -138^\circ$ in $f \leq 512 \text{ kHz}$. Therefore, the CryoSTM-TIA is stable with gain margin more than 10 dB and phase margin more than 42° .

2.5 Voltage gain and transimpedance gain of the proposed CryoSTM-TIA

With the compensated feedback network mentioned in Sect.2.3, it can be considered that Z_F is equal to R_F in $(0, 1 \text{ MHz}]$. Considering the TJ capacitance C_J , the TJ impedance should be $Z_J = R_J/(1 + j2\pi f R_J C_J)$. And, $C \approx C_A + C_I$. As the AC input voltage \dot{V}_i is applied by BMS, the output voltage of the CryoSTM-TIA is \dot{V}_o , and the voltage gain of the CryoSTM-TIA is $A_v = \dot{V}_o/\dot{V}_i$. In $(0, 1 \text{ MHz}]$, by the nodal analysis method, A_v is

$$A_v \approx -\frac{R_F}{Z_J} \cdot \frac{1}{1 - \frac{1}{a_A} - \frac{R_F}{a_A R_J} - \frac{R_F}{a_A R_A} - j2\pi f \frac{R_F(C_A + C_I)}{a_A}}. \quad (2.6)$$

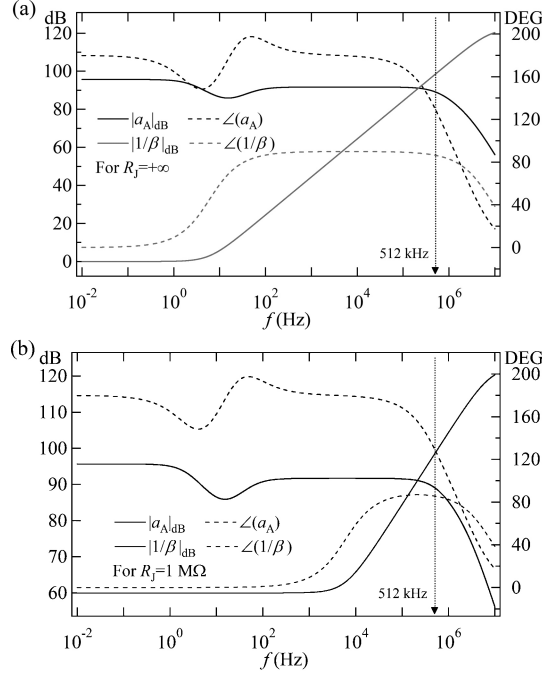


Figure 4: TINA-TI simulation results for the voltage gain Inv-Amp a_A , and $1/\beta(f)$ (a) with $R_J = +\infty$, (b) with $R_J = 1 \text{ M}\Omega$. Both figures show $|T_L|_{\text{dB}} = |a_A|_{\text{dB}} - |1/\beta(f)|_{\text{dB}} \leq -10$ dB in $f \geq 512$ kHz and $\angle(T_L) = \angle(-a_A) - \angle(1/\beta) = \angle(a_A) - 180^\circ - \angle(1/\beta) > -138^\circ$ in $f < 512$ kHz. Hence, the CryoSTM-TIA is stable enough.

Setting $\dot{V}_i = 0$ and applying a sinusoidal current source \dot{I}_i in parallel with TJ, the output voltage \dot{V}_o is generated at the output of the CryoSTM-TIA. $A_i = \dot{V}_o/\dot{I}_i$ is called as the transimpedance gain of the CryoSTM-TIA. In $(0, 1 \text{ MHz}]$, A_i is

$$A_i \approx -\frac{R_F}{1 - \frac{1}{a_A} - \frac{R_F}{a_A R_J} - \frac{R_F}{a_A R_A} - j2\pi f \frac{R_F(C_A + C_I)}{a_A}}. \quad (2.7)$$

Disconnecting TIA with the signal source circuit, and applying a sinusoidal current source \dot{I}_{iT} into the input of TIA, the output voltage \dot{V}_{oT} is generated at the output of TIA. $A_{iT} = \dot{V}_{oT}/\dot{I}_{iT}$ is called as the transimpedance gain of TIA. In $(0, 1 \text{ MHz}]$, A_{iT} is

$$A_{iT} = -\frac{R_F}{1 - \frac{1}{a_A} - \frac{R_F}{a_A R_A} - j2\pi f \frac{R_F C_A}{a_A}}, \quad (2.8)$$

In Fig.5, $|A_{iT}/R_F|_{\text{dB}}$ and $\angle(A_{iT}/R_F)$ calculated by Eq.(2.8) with the parameters in Table 1 is identical with their TINA-TI simulation results in $[1 \text{ kHz}, 1 \text{ MHz}]$, which verifies the correctness of Eq.(2.8) for A_{iT} . The upper cut-off frequency of $A_{iT}(f)/R_F$, i.e. its -3 dB frequency is $f_{hT} = 320$ kHz. Comparing Eq.(2.7) with Eq.(2.8), as $C_A + C_I + C_J \approx C_A + C_I \approx C_A$ and $R_J \geq 10^{-3}R_F$, the upper cut-off frequency of the CryoSTM-TIA is approximately equal to f_{hT} .

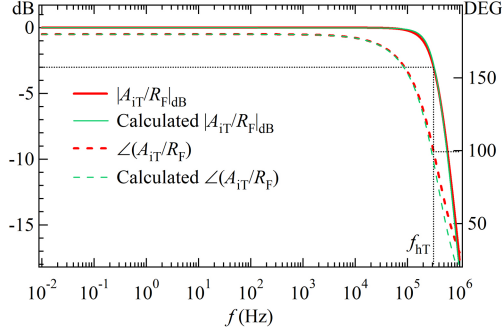


Figure 5: TINA-TI simulation results for A_{iT}/R_F , A_{iT} is the transimpedance gain of TIA in the proposed CryoSTM-TIA. $|A_{iT}(f_{hT})/R_F|_{dB} = -3$ dB and $\angle(A_{iT}(f_{hT})/R_F) = 99^\circ$ at $f_{hT} = 320$ kHz.

2.6 Transient response of the proposed CryoSTM-TIA

The simulation results for the transient response of the proposed CryoSTM-TIA are shown in Supplemental file 2 [24]. For the CryoSTM-TIA, the time taken from adding the input step signal voltage to the output response stably within a certain error is called transient response time t_r . For the simulations, a resistor with a constant resistance R_0 is instead of the tip-sample junction. When $R_0 \geq 30$ M Ω , for 0.1% error, $t_r < 5$ μ s. When 5 M $\Omega \leq R_0 < 30$ M Ω , for 1% error, $t_r < 5$ μ s. When 1 M $\Omega \leq R_0 < 5$ M Ω , for 3% error, $t_r < 5$ μ s.

3 Inherent noise of the proposed CryoSTM-TIA

For the circuit of the proposed CryoSTM-TIA shown in Fig.1, the differential equivalent circuit with all noise sources is used to calculate its equivalent input noise. The details for the noise calculations are shown in Supplemental file 3 [28].

3.1 Equivalent input voltage noise and equivalent input current noise of Inv-Amp

The equivalent input noise voltage and equivalent input noise current of C-H are denoted as e_H and i_H respectively. The resistors R_1 , R_2 , and R_f are in the cryogenic zone of 4.2 K, and their noises in $f > 1$ kHz are thermal noise, which can be neglected [3]. The thermal noise voltage of the resistor R_H is e_{RH} . The equivalent input noise voltage and equivalent input noise current of the Rear-OPA are denoted as e_a and i_a respectively. These noise sources are independent. The equivalent input noise voltage and equivalent input noise current of Inv-Amp are denoted as e_A and i_A respectively. By the nodal analysis method and Wiener-Sinichin theorem, ignoring the minor terms, it is obtained that

$$\overline{e_A^2} = \overline{e_H^2} + \frac{R_{HL}^2}{R_H^2} \frac{\overline{e_{RH}^2}}{A_{VP}^2} + \frac{\overline{e_a^2}}{A_{VP}^2} + \left(1 + \frac{R_{HL}}{R_d}\right)^2 \frac{\overline{i_a^2}}{g_m^2}, \quad (3.1)$$

$$\overline{i_A^2} = \overline{i_H^2} + (2\pi f)^2 \frac{C_A^2}{A_{VP}^2} \left(\frac{R_{HL}^2}{R_H^2} \overline{e_{RH}^2} + \overline{e_a^2} \right) + (2\pi f)^2 \left(C_{gs} + C_{gd} + \frac{R_{HL}}{R_d} C_A \right)^2 \frac{\overline{i_a^2}}{g_m^2}, \quad (3.2)$$

$$\begin{aligned} \overline{e_A i_A^*} = (\overline{i_A e_A^*})^* &= -j2\pi f \frac{C_A}{A_{VP}^2} \left(\frac{R_{HL}^2}{R_H^2} \overline{e_{RH}^2} + \overline{e_a^2} \right) \\ &\quad - j2\pi f \left(C_{gs} + C_{gd} + \frac{R_{HL}}{R_d} C_A \right) \left(1 + \frac{R_{HL}}{R_d} \right) \frac{\overline{i_a^2}}{g_m^2}. \end{aligned} \quad (3.3)$$

According to the parameters listed in Table 1, for Inv-Amp in this work, $\overline{e_A^2} = 0.27$ (nV)²/Hz and $\overline{i_A^2} = 0.13$ (fA)²/Hz at $f = 10$ kHz, and $\overline{e_A^2} = 0.08$ (nV)²/Hz and $\overline{i_A^2} = 2.7$ (fA)²/Hz at $f = 100$ kHz. For the Macro-OPA in Ref.[3], $\overline{e_A^2} = 0.5$ (nV)²/Hz and $\overline{i_A^2} = 0.8$ (fA)²/Hz at $f = 10$ kHz, and $\overline{e_A^2} = 0.14$ (nV)²/Hz and $\overline{i_A^2} = 20$ (fA)²/Hz at $f = 100$ kHz. The resistor R_H in Inv-Amp in this work replaces the transistor H2 in the Macro-OPA in Ref.[3]. The noise generated by R_H is 2 orders of magnitude smaller than that generated by H2 in the Macro-OPA in Ref.[3], i.e. $\overline{e_{RH}^2} \ll A_{VP}^2 \overline{e_H^2}$. Therefore, the equivalent input noises of Inv-Amp in this work are much lower than those of the Macro-OPA in Ref.[3].

In $f \geq 10$ kHz, $\overline{e_a^2} = 2.25$ (nV)²/Hz and $\overline{i_a^2} = 4$ (pA)²/Hz [17]. In Eqs.(3.1), (3.2), and (3.3), $\overline{e_{RH}^2} R_{HL}^2 / R_H^2$ is one order of magnitude smaller than $\overline{e_a^2}$. In Eq.(3.1), $(1 + R_{HL}/R_d)^2 \overline{i_a^2} / g_m^2$ is 2 orders of magnitude smaller than $\overline{e_H^2}$. In Eq.(3.2), $(C_{gs} + C_{gd} + C_A R_{HL}/R_d)^2 \overline{i_a^2} / g_m^2$ is one order of magnitude smaller than $C_A^2 \overline{e_a^2} / A_{VP}^2$. In Eq.(3.3), $(C_{gs} + C_{gd} + C_A R_{HL}/R_d) (1 + R_{HL}/R_d) \overline{i_a^2} / g_m^2$ is one order of magnitude smaller than $C_A \overline{e_a^2} / A_{VP}^2$. Further ignoring the minor terms in Eqs.(3.1), (3.2), and (3.3),

$$\overline{e_A^2} = \overline{e_H^2} + \overline{e_a^2} / A_{VP}^2, \quad (3.4)$$

$$\overline{i_A^2} = \overline{i_H^2} + (2\pi f)^2 C_A^2 \overline{e_a^2} / A_{VP}^2, \quad (3.5)$$

$$\overline{e_A i_A^*} = (\overline{i_A e_A^*})^* = -j2\pi f C_A \overline{e_a^2} / A_{VP}^2. \quad (3.6)$$

3.2 Equivalent input current noise of the proposed CryoSTM-TIA

The equivalent input noise current PSD of the proposed CryoSTM-TIA is obtained as

$$\begin{aligned} \overline{i_{in}^2} &= \overline{i_A^2} + 4k_B T / R_F + [1/R_J^2 + 1/R_F^2 + (2\pi f)^2 C_{IJ}^2] \overline{e_A^2} \\ &\quad + (1/R_J + j2\pi f C_{IJ}) \left(\overline{e_A i_A^*} + \overline{e_A^2} / R_F \right) \\ &\quad + (1/R_J - j2\pi f C_{IJ}) \left(\overline{i_A e_A^*} + \overline{e_A^2} / R_F \right), \end{aligned} \quad (3.7)$$

where $C_{IJ} = C_I + C_J$ [3, 25, 28]. Putting Eqs.(3.4), (3.5), and (3.6) into Eq.(3.7),

$$\begin{aligned} \overline{i_{in}^2} &= \overline{i_H^2} + 4k_B T / R_F + (1/R_J + 1/R_F)^2 \left(\overline{e_H^2} + \overline{e_a^2} / A_{VP}^2 \right) \\ &\quad + (2\pi f)^2 \left(C_{IJ}^2 \overline{e_H^2} + C^2 \overline{e_a^2} / A_{VP}^2 \right), \end{aligned} \quad (3.8)$$

i.e.

$$\overline{i_{in}^2} = \overline{i_A^2} + 4k_B T / R_F + (1/R_J + 1/R_F)^2 \overline{e_A^2} + \overline{i_{CIJ}^2}, \quad (3.9)$$

where $\overline{i_{\text{CIJ}}^2} = (2\pi f)^2(C_{\text{IJ}}^2 \overline{e_{\text{A}}^2} + 2C_{\text{A}}C_{\text{IJ}}\overline{e_{\text{a}}^2}/A_{\text{VP}}^2)$.

For the proposed CryoSTM-TIA, $R_{\text{F}} = 1 \text{ G}\Omega$, $C_{\text{A}} = 26 \text{ pF}$, $C_{\text{I}} = 0.5 \text{ pF}$, and $C_{\text{J}} = 10 \text{ fF}$. R_{F} and TJ are in the cryogenic zone at 4.2 K. As $R_{\text{J}} = 1 \text{ M}\Omega$, $\overline{i_{\text{in}}^2}$ and its four components are listed in Table 2. The noise components of the CryoSTM-TIA in Ref.[3] are also shown in Table 2. The CryoSTM-TIA proposed in this work has an equivalent input noise current PSD of $0.6 \text{ (fA)}^2/\text{Hz}$ at 10 kHz and $3 \text{ (fA)}^2/\text{Hz}$ at 100 kHz, which is much lower than that in Ref.[3].

Table 2: Noise components of CryoSTM-TIAs

Pre-Amp type	Single HEMT Amp		Pre-Amp in Ref.[3]	
$f \text{ (kHz)}$	10	100	10	100
$\overline{e_{\text{A}}^2} \text{ ((nV)}^2/\text{Hz})$	0.27	0.08	0.5	0.14
Unit for the following terms is $\text{(fA)}^2/\text{Hz}$				
$\overline{i_{\text{A}}^2}$	0.13	2.7	0.8	20
$4k_{\text{B}}T/R_{\text{F}}$	0.2	0.2	0.2	0.2
$\overline{i_{\text{CIJ}}^2}$	0.0013	0.06	0.03	0.7
$(\frac{1}{R_{\text{I}}} + \frac{1}{R_{\text{F}}})^2 \overline{e_{\text{A}}^2}$	0.26	0.08	0.5	0.14
$\overline{i_{\text{in}}^2}$ as total	0.6	3	1.5	21

For the Epi-wafer of the CNRS-HEMT, as Si is doped in $\text{Al}_x\text{Ga}_{1-x}\text{As}$, each dopant gives rise to two types of electronic states: a shallow and delocalized donor level associated with the normal substitutional site configuration, called as shallow donor state; a more localized acceptor level, known as DX^- center, arising from a lattice distortion. In $\text{Al}_x\text{Ga}_{1-x}\text{As}$, as $x > 0.22$, DX^- as a bound state is more stable than the shallow donor state. And, $x = 0.37$ for CNRS-HEMT in this work. There is a large repulsion barrier E_{cap} in the transition from the shallow donor to DX^- , so DX^- is frozen as $T < 120 \text{ K}$ [26, 27].

According to the work on the noise mechanism of the CNRS-HEMT [5], “bias-cooling method” can be used to control the density of the frozen DX^- centers in the doping area in the HEMT. This unique method, by which the in-situ modification of the HEMT structure is realized, can be used to reduce the noise generated by the HEMT. By cooling the HEMT with the positive gate-source voltage, more electrons in the HEMT are frozen into the DX^- centers. At low temperatures, the absolute of the gate-source voltage required to maintain the HEMT at the ideal operating point is reduced, so that the gate leakage current is reduced, and thus the low frequency noises generated by the gate leakage current is reduced [5]. By the means, the inherent noise of the CryoSTM-TIA can be reduced. Moreover, if the HEMT used for the CryoSTM-TIA is not CNRS-HEMT, or its noise performances are not as good as those listed in Table 1, it can be remedied by “bias-cooling method”. This approach is very convenient for cases with only a single HEMT in Pre-Amp.

4 Operating state adjustment and DC tunneling current measurements

For the CryoSTM-TIA in Fig.1, along with the circuit parameters listed in Table 1, its operating state can be adjusted as follows. (1) Disconnect Pre-Amp from Post-Amp and ground the input of Pre-Amp, i.e. gate G of C-H. Adjust R_{p2} to $R_{\text{p2}} = R_{\text{p1}}$. Adjust the

constant-current source to generate current as $I_{\text{sour}} = 2 \text{ mA}$. Adjust R_{s1} and R_{h1} to achieve C-H at the ideal operating point ($V_{ds} = 100 \text{ mV}$, $I_{ds} = 1 \text{ mA}$) and the potentials at O_1 and O_2 equal. That is to say, R_{s1} and R_{h1} are adjusted to realize $R_H = R_S + V_{ds}/I_{ds} = R_S + 100 \Omega$. (2) Cascade Pre-Amp and Post-Amp to form Inv-Amp, and input G is still grounded. By then, the DC output voltage V_{om} of Inv-Amp is usually not 0. V_{om} is induced by the input offset voltage of the Rear-OPA [17], its input bias currents and input offset current, and the common-mode DC voltages on the the inputs of the Rear-OPA. Adjust R_{h1} and R_{p2} to achieve the current through R_{p2} back to 1 mA and $V_{om} = 0$. Therefore, C-H is also at the ideal operating point. (3) Connect output O and input G of Inv-Amp with the feedback network and disconnect input G from ground, to form TIA. Input G is still not connected with the signal source circuit, so the potential of input G and output O of Inv-Amp is still 0, since the input resistance of the transistor C-H R_A can be considered as infinity. In the feedback network, $R_F + R_k \approx R_F = 1 \text{ G}\Omega$. (4) Connect the signal source circuit to TIA, to form the CryoSTM-TIA.

When $f \rightarrow 0$, $a_A \rightarrow a_{A0}$, and a_{A0} is the DC voltage gain of Inv-Amp. $|a_{A0}|_{\text{dB}} \approx (g_m R_f / g_d R_H)_{\text{dB}} \approx 96.4 \text{ dB}$, which is consistent with the simulation result $|a_{A0}|_{\text{dB}} = 95.6 \text{ dB}$ shown in Fig.2. As the DC bias V_i is applied by BMS, the DC resistance of TJ is R , and the potential at input G is V_G , and the output voltage of the CryoSTM-TIA is V_o . Obviously, $a_{A0} V_G = V_o$, and $(V_i - V_G)/R = (V_G - V_o)/R_F$. The DC bias on TJ is $V = V_i - V_G$, and the DC tunneling current $I = (V_i - V_G)/R$. I_s as an approximate value of I is

$$I_s = -V_o/R_F. \quad (4.1)$$

And, the relative error is obtained as

$$Er = |I_s - I|/|I| = 1/(1 - a_{A0}).$$

As $|a_{A0}|_{\text{dB}} \approx 96 \text{ dB}$, $Er < 20 \text{ ppm}$, consistent with the simulation results [29]. Since $a_{A0} V_G = V_o$, the DC bias on TJ is

$$V = V_i - V_o/a_{A0}. \quad (4.2)$$

By Eq.(4.1), $V_o = -R_F I_s \approx -R_F I = -R_F V/R$. By Eq.(4.2), $V_i \approx V - R_F V/(R a_{A0})$. As the minimum of R_J is not less than $1 \text{ M}\Omega$, $R \geq 1 \text{ M}\Omega$, so $|R_F/(R a_{A0})| \leq 1/60$. Thus, $V \approx V_i$. With the measured V_o , $I \approx I_s$ and $V \approx V_i$ can be obtained. Therefore, the scanning tunneling current spectra $I = I(V)$ ($V \in [V_L, V_H]$) can be obtained, where V_L and V_H are the lower limit and upper limit voltages for the measurements respectively.

It should be noted that Pre-Amp in this work is not a differential structure, so there is no function for it to counteract the influences of the temperature drift as that for the differential structure. The drift of V_{om} can be considered as the amplification of the drift of the Inv-Amp input offset voltage V_{OS} , where $V_{om} = a_{A0} V_{OS}$. The estimated drift of $|V_{OS}|$ is about $0.5 \text{ mV}/^\circ\text{C}$ [30]. The power of the constant-current source is about 24 mW . The well-designed temperature Control System based on the TEC devices [31] can be used to control the temperature fluctuations of the constant-current source within $0.0002 \text{ }^\circ\text{C}$ [33] and those of Rear-OPA within $0.1 \text{ }^\circ\text{C}$, so the fluctuations of V_{OS} within 150 nV is guaranteed, i.e. the TIA output fluctuations within 150 nV [3].

In order to prove the correctness of our proposed method for designing TIA, the N-Channel JFET (SST4393) is chosen to replace CNRS-HEMT, and TIA is designed and

fabricated with the same circuit design method and the same circuit topology. SST4393 can work at 77 K. We measured the gain, noise, and transient response of JFET-based Inv-Amp and TIA at room temperature and 77 K [32]. The experimental results are basically consistent with the theoretical calculations and simulations, which shows that the method of designing TIA is correct. In addition, the designed JFET-based TIA can also be used for STM at 77 K, with larger bandwidth and lower inherent noise, comparing with traditional TIAs for CryoSTM (e.g. FEMTO DE-DLPCA-200 TIA).

5 Applications for the proposed CryoSTM-TIA in spectra measurements

For most applications, the modulus of the transimpedance gain of the CryoSTM-TIA $|A_i(f)|$ should be measured firstly. $A_i(f)$ is expressed as Eq.(2.7). Since $|a_A(f)|_{\text{dB}} > 90$ dB in [1 kHz, 300 kHz] as shown in Fig.2, when $R_J \geq 10^{-3}R_F$, $|A_i(f)|$ in [1 kHz, 300 kHz] can be approximately expressed as

$$|A_i(f)| = R_F / |1 - j2\pi f R_F (C_A + C_I) / a_A(f)|. \quad (5.1)$$

How to measure it has been described in Ref.[3].

5.1 Measurements of scanning tunneling differential conductance spectra by the proposed CryoSTM-TIA

The differential conductance of TJ $G_J = 1/R_J$ is the function of the voltage V applied to TJ. As the frequency f of the modulated signal voltage \dot{V}_i provided by BMS is low enough, such as $f < 1$ kHz, by Eq.(2.6),

$$A_v \approx \frac{R_F}{R_J(V)} \cdot \frac{1}{1 - \frac{R_F}{a_A(f)R_J(V)}}.$$

Therefore, $R_J(V) \approx [1/A_v + 1/a_A(f)] R_F$. When the measured $|A_v| \leq 1000$, $R_J(V) \approx R_F/|A_v|$, since $|a_A(f)|_{\text{dB}} \geq 85$ dB in $f \leq 300$ kHz as shown in Fig.2. With the measured $|A_v| = |\dot{V}_o|/|\dot{V}_i|$, the differential conductance spectra $G_J(V) = 1/R_J(V)$ ($V \in [V_L, V_H]$) can be obtained.

Increasing the frequency f of the modulated signal can speed up the scanning tunneling differential conductance spectra measurements. In [1 kHz, 300 kHz], as $R_J \geq 1 \text{ M}\Omega$, by Eq.(2.6),

$$|A_v(f)| \approx \frac{1}{|Z_J(f)|} \cdot \frac{R_F}{|1 - j2\pi f R_F (C_A + C_I) / a_A(f)|}.$$

Therefore, $1/|Z_J(f)| \approx |A_v(f)|/|A_i(f)|$, where $|A_i(f)|$ is shown by Eq.(5.1). And, $|A_v(f)|$ and $|A_i(f)|$ can be measured. $1/|Z_J(f)| = \sqrt{1/R_J^2 + (2\pi f C_J)^2}$ can be obtained. Selecting two different frequencies f_1 and f_2 in [1 kHz, 300 kHz], $|Z_J(f_1)|$ and $|Z_J(f_2)|$ are obtained. R_J and C_J can be solved out from the measured $|Z_J(f_1)|$ and $|Z_J(f_2)|$.

Since the inherent noise of the CryoSTM-TIA is very small, the amplitude of the modulated signal voltage \dot{V}_i can be very small ($\leq 10 \text{ }\mu\text{V}$), so that the energy resolution for STS is much improved.

5.2 Measurements of scanning tunneling shot noise spectra by the proposed CryoSTM-TIA

The measurement method for the tunneling shot noise spectra by the proposed CryoSTM-TIA is basically the same as that introduced by Ref.[3], and it is only briefly described here.

Before approaching the tip to the sample in the CryoSTM, R_J can be considered as infinity and C_J as 0. In this case, the output noise voltage PSD of the CryoSTM-TIA $S_{\text{su}}(f)$ can be measured, and the equivalent input noise current PSD $\overline{i_i^2}(f)$ is

$$\overline{i_i^2}(f) = S_{\text{su}}(f)/|A_i(f)|^2, \quad (5.2)$$

where $|A_i(f)|$ is obtained by Eq.(5.1).

To measure the scanning tunneling shot noise spectra (STSNS) of a quantum system by the CryoSTM-TIA, the distance between the tip and sample is adjusted, and the interval $[V_L, V_H]$ is selected, so that the shot noise measurements at $V \in D_V = \{V | V_L \leq V \leq V_H, G_J(V) < 1 \mu S\}$ are needed to study the physical properties of the quantum system [3]. In D_V , the output noise voltage PSD $S_{\text{sum}}(f, V)$ can be measured. The tunneling noise current PSD is denoted as $S_I(f, V)$. The equivalent input noise current PSD of the CryoSTM-TIA is the function of R_J , so it is the function of V and denoted as $\overline{i_{\text{in}}^2}(f, V)$. For $S_{\text{sum}}(f, V)$,

$$S_{\text{sum}}(f, V) = [S_I(f, V) + \overline{i_{\text{in}}^2}(f, V)] \cdot |A_i(f)|^2. \quad (5.3)$$

With Eq.(5.2) and (5.3), it is obtained that

$$S_I(f, V) = \frac{S_{\text{sum}}(f, V) - S_{\text{su}}(f)}{|A_i(f)|^2} - [\overline{i_{\text{in}}^2}(f, V) - \overline{i_i^2}(f)]. \quad (5.4)$$

From Eq.(3.9),

$$\overline{i_i^2}(f) = \overline{i_A^2} + \frac{4k_B T}{R_F} + \frac{\overline{e_A^2}}{R_F^2} + (2\pi f)^2 \left(C_I^2 \overline{e_A^2} + 2C_A C_I \frac{\overline{e_a^2}}{A_{\text{vp}}^2} \right).$$

And, $\overline{i_{\text{in}}^2}(f, V)$ is composed by the four parts as shown in Eq.(3.9). According to Table 2, $\delta(f, V)$ as the difference between $\overline{i_{\text{in}}^2}(f, V)$ and $\overline{i_i^2}(f)$ is smaller than $0.3 \text{ (fA)}^2/\text{Hz}$ in $[10 \text{ kHz}, 100 \text{ kHz}]$ and $0.1 \text{ (fA)}^2/\text{Hz}$ in $[100 \text{ kHz}, 300 \text{ kHz}]$. $\delta(f, V)$ can be neglected compared with $S_I(f, V)$, so long as the minimum of $G_J(V)$ ($V \in D_V$) is not too small. Therefore, $S_I(f, V)$ can be obtained as

$$S_I(f, V) \approx \frac{S_{\text{sum}}(f, V) - S_{\text{su}}(f)}{|A_i(f)|^2}, \quad (5.5)$$

by the measured $S_{\text{sum}}(f, V)$, $S_{\text{su}}(f)$, and $|A_i(f)|$. And then, the SNTNS $S_{\text{Is}}(I) = 2Fe|I|$ can be extracted from $S_I(f, V)$. Here, $I = I(V)$ ($V \in D_V$), and I is the DC tunneling current as the bias V is applied.

Compared with the CryoSTM-TIA in Ref.[3], the CryoSTM-TIA proposed in this work has the same bandwidth and transimpedance gain, but its inherent noise is much lower. The inherent noise of the CryoTM-TIA in this work is only $3 \text{ (fA)}^2/\text{Hz}$ at 100 kHz

and its $\delta(f, V) < 0.1 \text{ (fA)}^2/\text{Hz}$ at 100 kHz, while that of the apparatus in Ref.[3] is $21 \text{ (fA)}^2/\text{Hz}$ at 100 kHz and $\delta(f, V) < 0.28 \text{ (fA)}^2/\text{Hz}$ at 100 kHz. Therefore, as investigating novel quantum states of various quantum systems, the measurements performed with the apparatus proposed in this work is more accurate.

For example, as investigating the existence of MBS in a magnetic flux vortex of the iron superconductor in CryoSTM [4], the tunnel junction resistance must be large enough, since the occurrence of incoherent Andreev reflection can be ruled out by weak tunnel coupling conditions [34]. In Ref.[4], the tunneling current I is quite low (see Fig.3(a) in Ref.[4] and Fig.S1(a) and (b) in its supplemental file). As the tunnel junction bias V is 0.3 mV, I is only tens of pA, and the corresponding shot noise may only be only a few $\text{(fA)}^2/\text{Hz}$. For the shot noise measurements in the system in Ref.[4], it is obvious that the CryoSTM-TIA proposed in this work is much more effective and accurate than that in Ref.[3].

6 Conclusion

In this work, a design of transimpedance amplifier (TIA) for cryogenic scanning tunneling microscope (CryoSTM) is presented. TIA connected with the tip-sample component in CryoSTM is called as CryoSTM-TIA. The CryoSTM-TIA in this work has transimpedance gain of $1 \text{ G}\Omega$ and bandwidth more than 300 kHz, and its equivalent input noise current PSD is only $3 \text{ (fA)}^2/\text{Hz}$ at 100 kHz. In this CryoSTM-TIA, a single CNRS-HEMT Pre-Amp is instead of the differential Pre-Amp consisting of a pair of CNRS-HEMTs in Ref.[3]. The difficulty of matching the identical HEMTs is avoided. And, due to the reduction of a noisy HEMT, the apparatus inherent noise is only 1/7 of that in Ref.[3]. Furthermore, the inherent noise of the single HEMT in the circuit can be in-situ reduced by “bias-cooling method”. With this apparatus, the fast high-energy-resolution scanning tunneling spectra measurements can be performed and the very low tunneling shot noise of quantum systems can be measured at the atomic scale. This apparatus can be applied to investigate novel physical properties of various quantum systems, such as detecting the existence of Majorana bound states in the topological quantum systems.

Acknowledgment

This work is supported by Open Research Fund Program of the State Key Laboratory of Low-Dimensional Quantum Physics (Grant No. KF202212). I acknowledge stimulating discussions with Prof. Fang-Hao Liang of Math School in Shandong Univ and Prof. Xing Liang of Math School in USTC.

Declaration of competing interest

The author declares that they have no known competing financial interests or personal relationships that could have appeared to influence the work reported in this paper.

References

- [1] C.J. Chen, Introduction to scanning tunneling microscopy, Oxford Univ. Press, (1993).
- [2] J.F. Ge, M. Ovadia, and J.E. Hoffman, Achieving low noise in scanning tunneling spectroscopy, Rev. Sci. Instrum. 90 (2019) 101401, <https://doi.org/10.1063/1.5111989>.
- [3] Y.X. Liang, Low-noise large-bandwidth transimpedance amplifier for measuring scanning tunneling shot noise spectra in cryogenic STM and its applications, Ultramicroscopy 234 (2022) 13466, <https://doi.org/10.1016/j.ultramic.2022.113466>.
- [4] D.F. Wang, L.Y. Kong, P. Fan, H. Chen, S.Y. Zhu, W.Y. Liu, L. Cao, Y.J. Sun, S.X. Du, J. Schneeloch, R.D. Zhong, G.D. Gu, L. Fu, H. Ding, and H.J. Gao, Evidence for Majorana bound states in an iron-based superconductor, Science 362 (2018) 333, <https://doi.org/10.1126/science.aao1797>.
- [5] Y.X. Liang, Q. Dong, M.C. Cheng, U. Gennser, A. Cavanna, and Y. Jin, Insight into low frequency noise induced by gate leakage current in AlGaAsGaAs high electron mobility transistors at 4.2 K, Appl. Phys. Lett. 99 (2011) 113505, <https://doi.org/10.1063/1.3637054>.
- [6] Y. Jin, Q. Dong, A. Cavanna, U. Gennser, L. Couraud, and C. Ulysse, Ultra-low noise HEMTs for deep cryogenic low-frequency and highimpedance readout electronics, 12th IEEE International Conference on Solid-State and Integrated Circuit Technology (ICSICT) (2014).
- [7] K.M. Bastiaans, D. Cho, T. Benschop, I. Battisti, Y. Huang, M.S. Golden, Q. Dong, Y. Jin, J. Zaanen, and M.P. Allan, Charge trapping and super-Poissonian noise centres in a cuprate superconductor, Nat. Phys. 14 (2018) 1183, <https://doi.org/10.1038/s41567-018-0300-z>.
- [8] F. Massee, Y.K. Huang, M.S. Golden, and M. Aprili, Noisy defects in the high- T_c superconductor $\text{Bi}_2\text{Sr}_2\text{CaCu}_2\text{O}_{8+x}$, Nat. Commun. 10 (2019) 544, <https://doi.org/10.1038/s41467-019-08518-1>.
- [9] C.J. Bolech and E. Demler, Observing majorana bound states in p-wave superconductors: using noise measurements in tunneling experiments, Phys. Rev. Lett. 98 (2007) 237002, <https://doi.org/10.1103/PhysRevLett.98.237002>.
- [10] A. Golub and B. Horovitz, Shot noise in a Majorana fermion chain, Phys. Rev. B 83 (2011) 153415, <https://doi.org/10.1103/PhysRevB.83.153415>.
- [11] H. Soller and A. Komnik, Charge transfer statistics of transport through Majorana bound states, Physica E 63 (2014) 99, <https://doi.org/10.1016/j.physe.2014.05.020>.
- [12] C.W.J. Beenakker and D.O. Oriekhov, Shot noise distinguishes Majorana fermions from vortices injected in the edge mode of a chiral p-wave superconductor, SciPost Phys. 9 (2020), 080, <https://doi.org/10.21468/SciPostPhys.9.5.080>.

- [13] K.M. Bastiaans, D. Cho, D. Chatzopoulos, M. Leeuwenhoek, C. Koks, and M.P. Allan, Imaging doubled shot noise in a Josephson scanning tunneling microscope, *Phys. Rev. B* 100 (2019) 104506, <https://doi.org/10.1103/PhysRevB.100.104506>.
- [14] K.M. Bastiaans, D. Chatzopoulos, J.F. Ge, D. Cho, W.O. Tromp, J.M. van Ruitenbeek, M.H. Fischer, P.J. de Visser, D.J. Thoen, E.F.C. Driessen, T.M. Klapwijk, and M.P. Allan, Direct evidence for Cooper pairing without a spectral gap in a disordered superconductor above T_c , *Science* 374 (2021) 608. <https://doi.org/10.1126/science.abe3987>.
- [15] S. Cocklin and D.K. Morr, Scanning tunneling shot-noise spectroscopy in Kondo systems, *Phys. Rev. B* 100 (2019) 125146, <https://doi.org/10.1103/PhysRevB.100.125146>.
- [16] Data sheet of BFT93 BJT, <https://www.nxp.com.cn/docs/en/datasheet/BFT93CNV.pdf>.
- [17] Data sheet of THS4021 OPA, <https://www.ti.com/lit/ds/symlink/ths4021.pdf>.
- [18] Data sheet of HF-STM-broadband cryogenic buffer amplifier made by Stahl-electronics, https://www.stahl-electronics.com/devices/hfstm/Datasheet_HF-STM1-E3a_v1.5.pdf. The input capacitance of this amplifier, including the input capacitance of the HEMT and the capacitance of the wire between the tip and the HEMT input, is only 2.7–3.1 pF. Therefore, $C_1 \leq 0.5$ pF is reasonable.
- [19] TINA-TI is SPICE-based analog simulation program produced by Texas Instruments Inc., <https://www.ti.com/tool/TINA-TI>.
- [20] Supplemental file 1.
- [21] Supplemental file 2.
- [22] B. Michel, L. Novotny, and U. Dürig, *Ultramicroscopy* 42-44 (1992) 1647,
- [23] S. Franco, *Design with Operational Amplifiers and Analog Integrated Circuits*, McGraw-Hill Companies, Inc., (2002).
- [24] Supplemental file 3.
- [25] A. van der Ziel, *Noise in solid state devices and circuits*, Wiley-Inter-Science, New York, (1986).
- [26] D.J. Chadi and K.J. Chang, Energetics of DX-center formation in GaAs and $\text{Al}_x\text{Ga}_{1-x}\text{As}$ alloys, *Phys. Rev. B* 39 (1989) 10063, <https://doi.org/10.1103/PhysRevB.39.10063>.
- [27] W.F. Li, Y.X. Liang, Y. Jin, and J.H. Wei, Bipolaron mechanism of DX center in $\text{Al}_x\text{Ga}_{1-x}\text{As}$: Si, *Acta. Phys. Sin.* 59 (2010) 8850, <https://doi.org/10.7498/aps.59.8850>.
- [28] Supplemental file 4.

- [29] Supplemental file 5.
- [30] Supplemental file 6.
- [31] A suitable TEC device, <https://datasheets.maximintegrated.com/en/ds/MAX1978-MAX1979.pdf>.
- [32] Paper is in preparation.
- [33] W. Zhang, Z.L. Li, P. Guo, and J.Y. Zhao, Design of precise temperature control system for saturated absorption Frequency stabilization of DFB Laser, *Semicond. Optoelectron.*, 41 (2020) 560, <https://doi.org/10.16818/j.issn1001-5868.2020.04.021>.
- [34] L.Y. Kong and H. Ding, Emergent vortex Majorana zero mode in iron-based superconductors, *Acta. Phys. Sin.*, 69 (2020) 110301, <https://doi.org/10.7498/aps.69.20200717>.

Supplemental file 1: Voltage gain of Inv-Amp

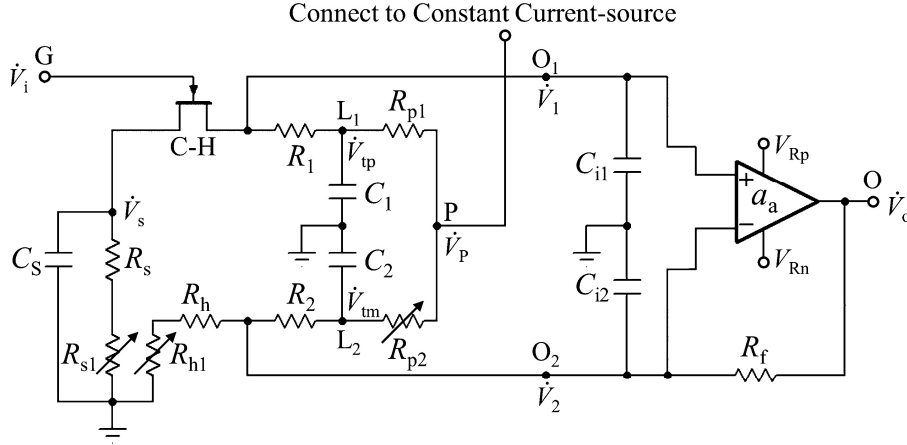


Figure s1-1 The Inv-Amp circuit with all components for Eqs.(s1.1-s1.8), and their values are shown in Table 1 in Article.

With the nodal analysis method, the Inv-Amp voltage gain $a_A(f)$ is calculated by the following equations. All components for Eqs.(s1.1-s1.8) are shown in Fig.s1-1, and their values are shown in Table 1 in Article.

$$(\dot{V}_o - \dot{V}_2)/R_f = (\dot{V}_2 - \dot{V}_{tm})/R_2 + \dot{V}_2/(R_h + R_{h1}) + j\omega C_{i2}\dot{V}_2 \quad , \quad (s1.1)$$

$$j\omega C_{gd}(\dot{V}_i - \dot{V}_1) = g_m(\dot{V}_i - \dot{V}_s) + g_d(\dot{V}_1 - \dot{V}_s) + (\dot{V}_1 - \dot{V}_{tp})/R_1 + j\omega C_{i1}\dot{V}_2 \quad , \quad (s1.2)$$

$$(\dot{V}_1 - \dot{V}_{tp})/R_1 = (\dot{V}_{tp} - \dot{V}_p)/R_{p1} + j\omega C_1\dot{V}_{tp} \quad , \quad (s1.3)$$

$$(\dot{V}_2 - \dot{V}_{tm})/R_2 = (\dot{V}_{tm} - \dot{V}_p)/R_{p2} + j\omega C_1\dot{V}_{tm} \quad , \quad (s1.4)$$

$$(\dot{V}_{tp} - \dot{V}_p)/R_{p1} + (\dot{V}_{tm} - \dot{V}_p)/R_{p2} = 0 \quad , \quad (s1.5)$$

$$g_m(\dot{V}_i - \dot{V}_s) + g_d(\dot{V}_1 - \dot{V}_s) = \dot{V}_s/R_s + j\omega C_s\dot{V}_s + j\omega C_{gs}(\dot{V}_s - \dot{V}_i) \quad , \quad (s1.6)$$

$$\dot{V}_o = a_a(\dot{V}_1 - \dot{V}_2) \quad , \quad (s1.7)$$

$$a_A = \dot{V}_o/\dot{V}_i \quad , \quad (s1.8)$$

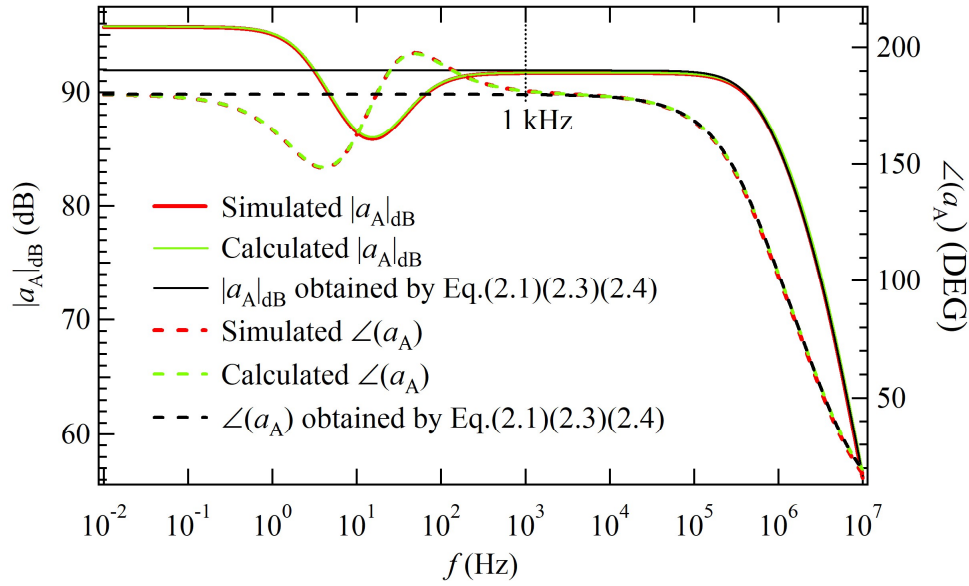


Figure s1-2 The Inv-Amp voltage gain $a_A(f)$. The solid curves are the curves of $|a_A(f)|_{\text{dB}}$, and the dashed curves are the curves of $\angle(a_A(f))$. The red curves are the TINA-TI simulation results, the green curves are the calculated results with the nodal analysis method (i.e. Eqs.(s1.1-1.8)), and the black curves are the calculated results by Eqs.(2.1), (2.3), and (2.4) in Article.

Fig. s1-2 shows the modulus of the Inv-Amp voltage gain $|a_A(f)|_{\text{dB}}$. The red solid curve is the TINA-TI simulation results, and the green solid curve is the calculated results with the nodal analysis method. They are identical with each other. The black solid curve is the calculated results by Eqs.(2.1), (2.3), and (2.4) in Article. In $f \in [1 \text{ kHz}, 3 \text{ MHz}]$, three curves are identical with one another.

Fig. s1-2 also shows the argument of the Inv-Amp voltage gain $\angle(a_A(f))$. The red dashed curve is the TINA-TI simulation results, and the green dashed curve is the calculated results with the nodal analysis method. They are identical with each other. The black dashed curve is the calculated results by Eq.(2.1), (2.3), and (2.4) in Article. In $f \in [1 \text{ kHz}, 3 \text{ MHz}]$, three curves are consistent with one another.

Supplemental file 2: Voltage gain peaks for cables

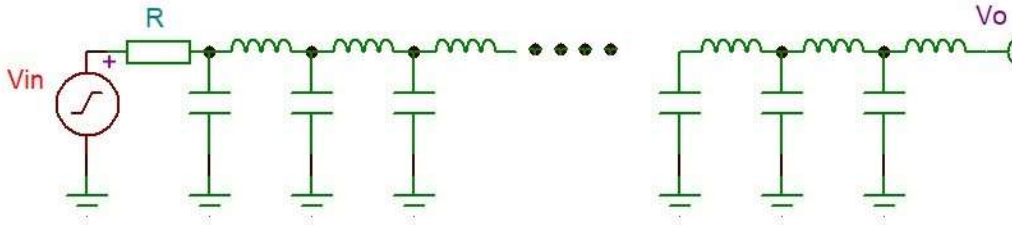


Figure s2-1 The circuit scheme for measuring the voltage gain peaks for cables.

A 1 meter cable with characteristic impedance of $50\ \Omega$ has a distributed capacitance of $100\ \text{pF}$ and a distributed inductance of $250\ \text{nH}$, which is shown as Fig. s2-1. In Fig. s2-1, $R=1.5\ \text{k}\Omega$, the gain is V_o/V_{in} . The simulation results show its distributed LC structure results in several resonant gain peaks in $[80\ \text{MHz}, 1\ \text{GHz}]$ shown as Fig. s2-2. We amplify V_o with Amplifier SA-220F5 (gain=200, $f_{in}=200\ \text{MHz}$), and then the gain peaks for the cable are measured with an oscilloscope. Fig. s2-3 show the measured gain peaks for cable.

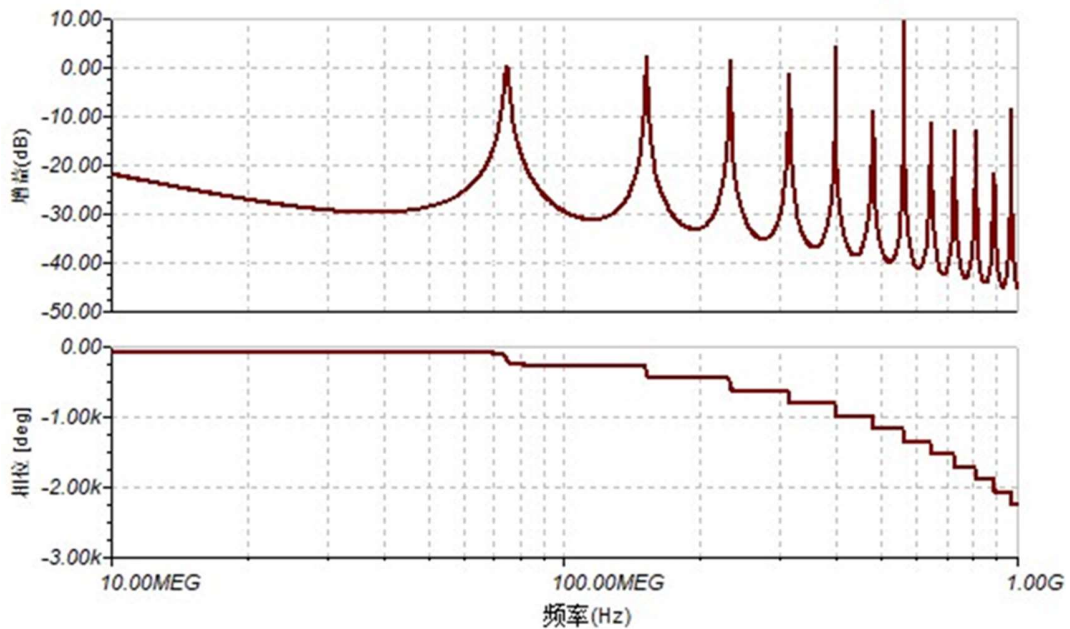


Figure s2-2 The simulation results of the gain peaks for a 1 meter cable with a distributed capacitance of $100\ \text{pF}$ and a distributed inductance of $250\ \text{nH}$.

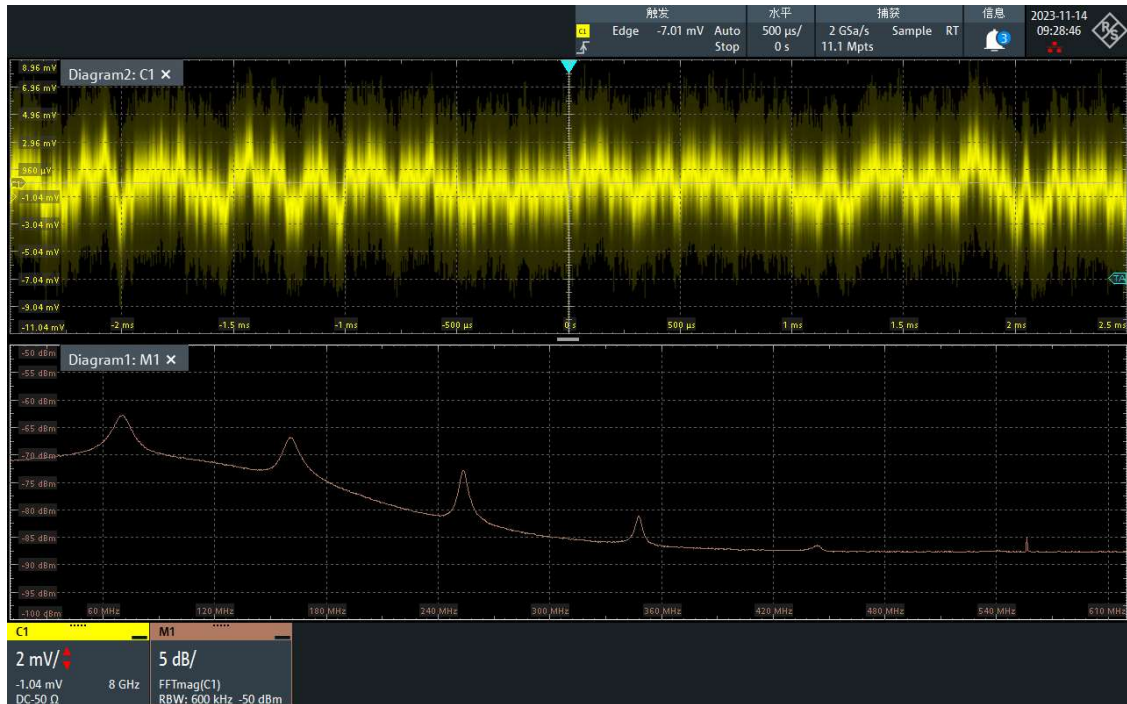


Figure s2-2 The measured results of the gain peaks for a 1 meter cable with a distributed capacitance of 100 pF and a distributed inductance of 250 nH.

Supplemental file 3: Transient response of the proposed CryoSTM-TIA

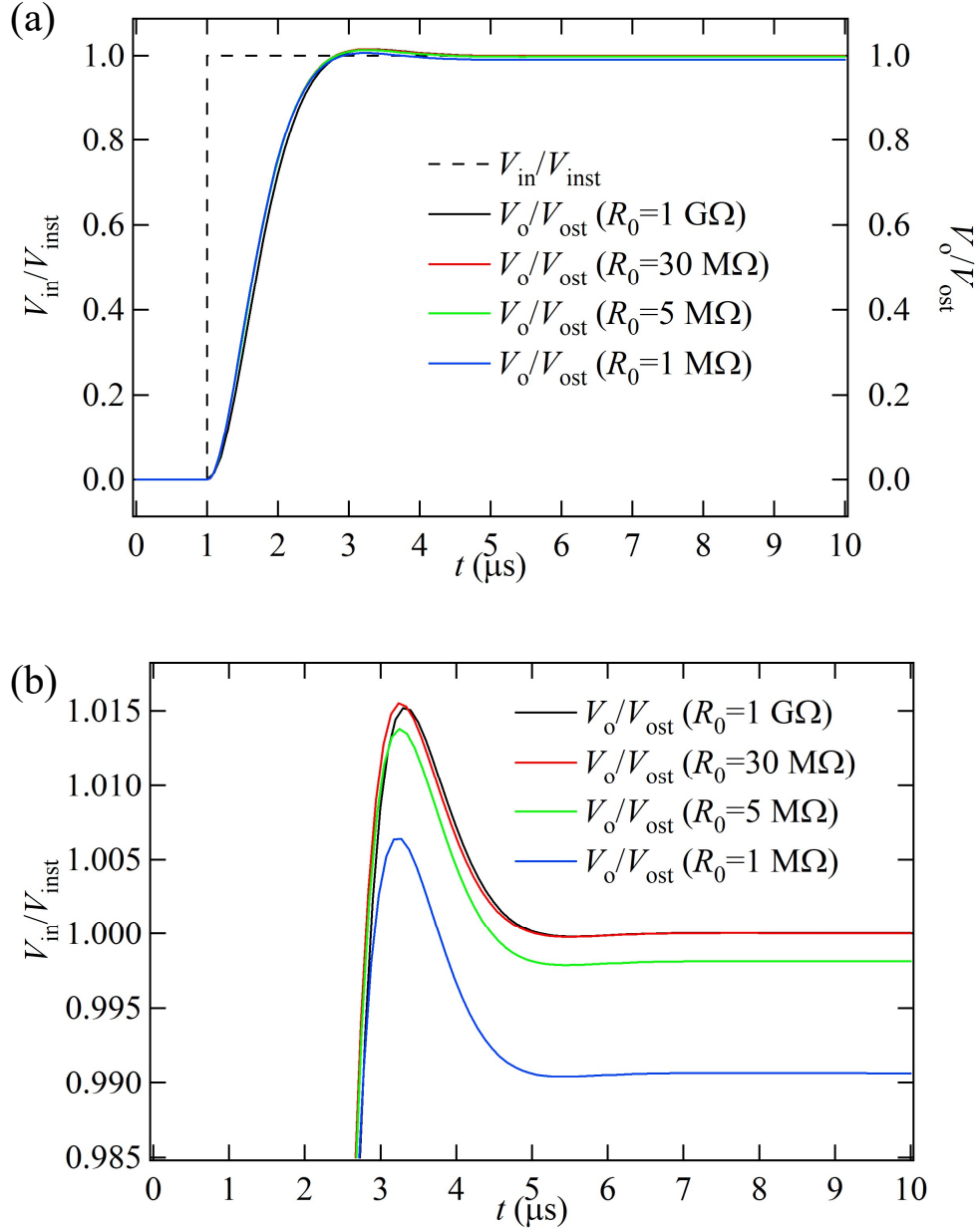
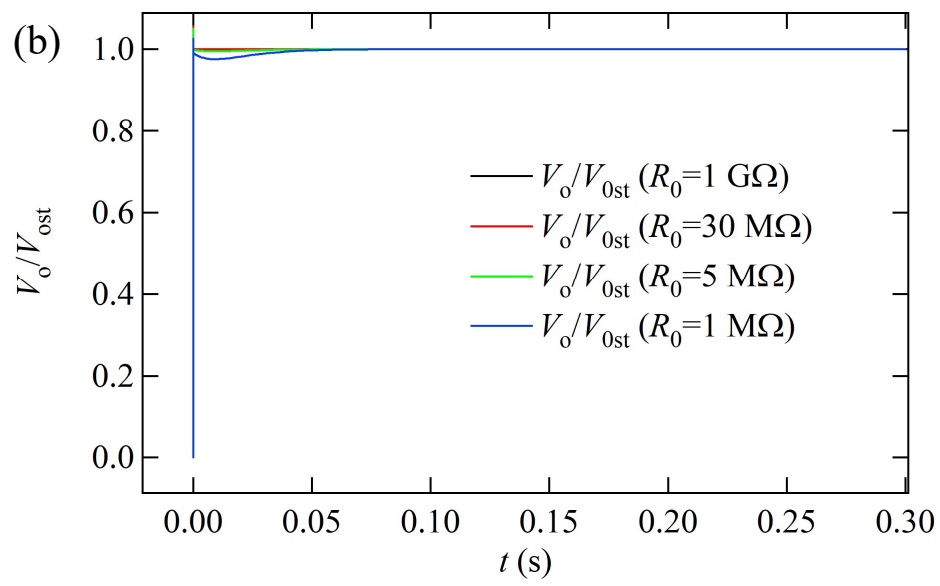
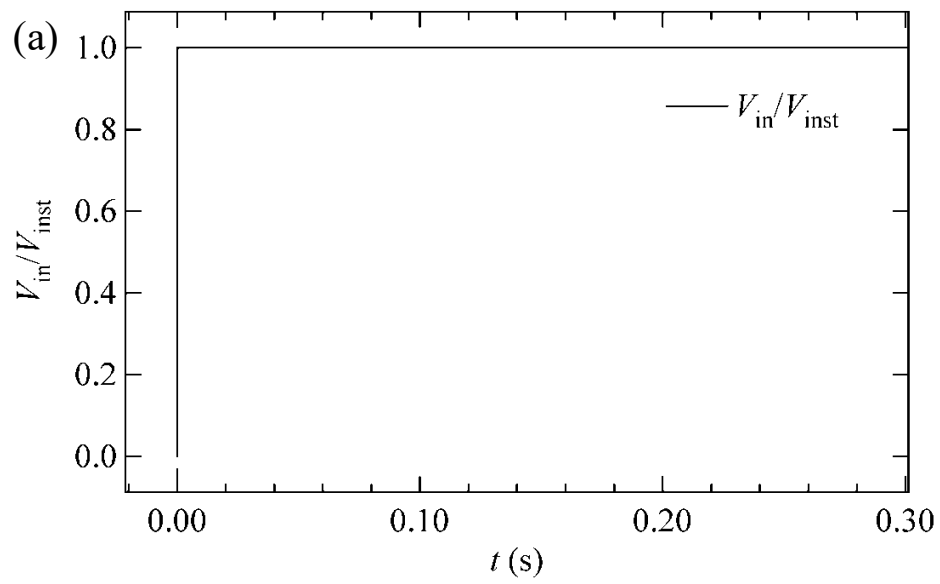


Figure s3-1 A resistor with a constant resistance R_0 is instead of the tip-sample junction for the simulation. TINA-TI simulation results for the transient response of the CryoSTM-TIA with the different R_0 for the time interval of 10 μs . The dashed curve is the step input signal V_i/V_{inst} for the different R_0 . The solid curves are the output response V_o/V_{ost} . Here, V_{ost} and V_{inst} are their values respectively at 300 ms after applying the step input signal V_i , which are shown in Fig.s2-2. Transient response time $t_r < 5 \mu s$. (b) is the zoom-in for the output response V_o/V_{ost} in (a).



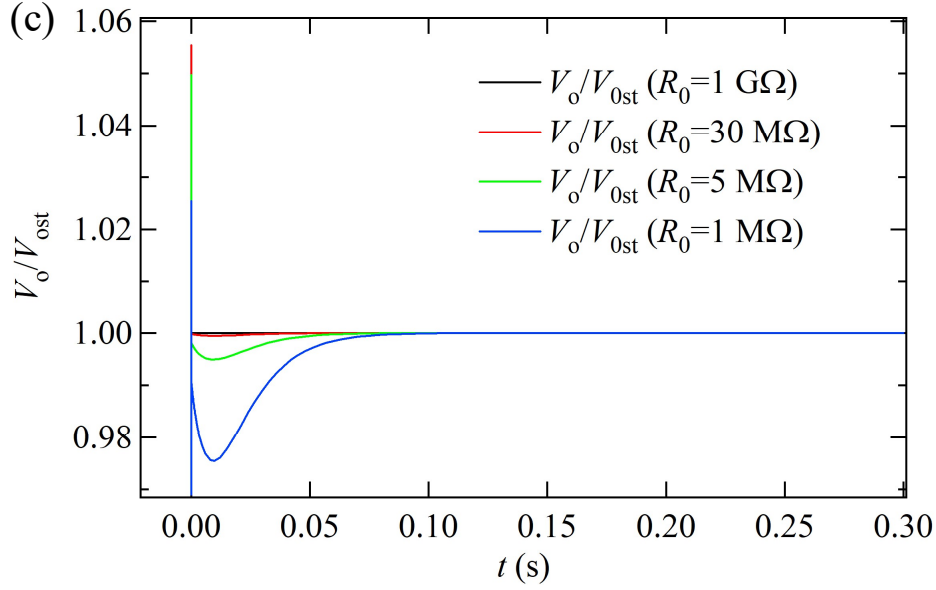


Figure s3-2 A resistor with a constant resistance R_0 is instead of the tip-sample junction for the simulation. TINA-TI simulation results for the transient response of the CryoSTM-TIA with different R_0 for the time interval of 300 ms. (a) The step input signal V_i/V_{inst} . (b) The output response V_o/V_{ost} . $V_o/V_{\text{ost}} = 1$ in $t \geq 100$ ms. (c) is the zoom-in figure of (b).

A resistor with a constant resistance R_0 is instead of the tip-sample junction for the simulation. Fig.s3-1 shows TINA-TI simulation results for the transient response of the CryoSTM-TIA with the different R_0 for the time interval of 10 μs . The dashed curve is the step input signal V_i/V_{inst} , and the solid curves are the output response V_o/V_{ost} for the different R_0 . Here, V_{ost} and V_{inst} are their values respectively at 300 ms after applying the step input signal V_i . The error is definite as $|V_o - V_{\text{ost}}|/|V_{\text{ost}}|$. For the CryoSTM-TIA, the time taken from adding the input step signal voltage to the output response stably within a certain error is called transient response time t_r . As shown in Fig.s3-1 and Fig.s3-2(b)&(c), with $R_0 = 1 \text{ G}\Omega$ and $30 \text{ M}\Omega$, for 0.1% error, $t_r < 5 \mu\text{s}$. With $R_0 = 5 \text{ M}\Omega$, for 1% error, $t_r < 5 \mu\text{s}$. And, With $R_0 = 1 \text{ M}\Omega$, for 2.5% error, $t_r < 5 \mu\text{s}$.

Supplemental file 4: Noise of the proposed CryoSTM-TIA

S4.1 Noises of STM-TIA

For Inv-Amp Inv as shown in Fig.s1-1, the equivalent input noise voltage of the Inv-Amp is denoted as e_A and its equivalent input noise current is i_A , and their harmonic components of frequency f are E_A and I_A respectively. $\begin{pmatrix} E_A \\ I_A \end{pmatrix}$ can be obtained by the nodal analysis method. By

Wiener-Khintchine theorem, $\begin{pmatrix} \overline{e_A^2} & \overline{e_A i_A^*} \\ \overline{i_A e_A^*} & \overline{i_A^2} \end{pmatrix}$ can be obtained from $\begin{pmatrix} E_A E_A^* & E_A I_A^* \\ I_A E_A^* & I_A I_A^* \end{pmatrix}$ [S4R1, S4R2].

The two matrix elements on the main diagonal are the equivalent input noise voltage PSD of the Inv-Amp $\overline{e_A^2}$ and its equivalent input noise current PSD $\overline{i_A^2}$. The two matrix elements on the sub-diagonal are its equivalent input noise voltage-current PSD $\overline{e_A i_A^*}$ and equivalent input noise current-voltage PSD $\overline{i_A e_A^*}$.

The Inv-Amp is connected to the feedback resistor R_F to form a TIA. The equivalent input noise voltage of the TIA is denoted as e_T and its equivalent input noise current is i_T , and their harmonic components of f are E_T and I_T respectively. The temperature of the feedback resistance R_F is T , and its noise voltage is e_F and its harmonic component of f is E_F .

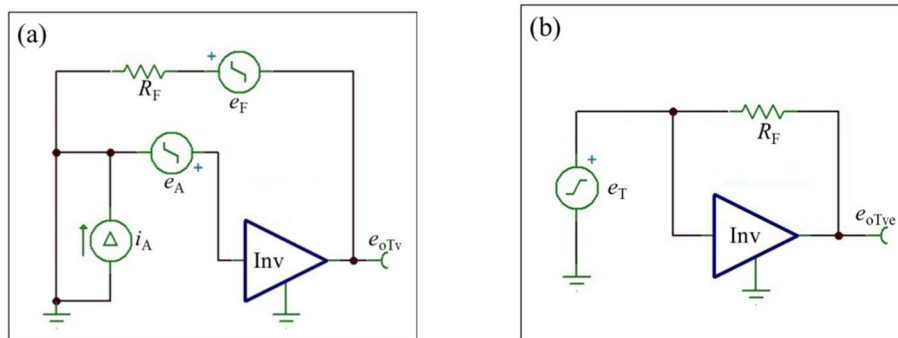


Figure s4-1 (a) TIA circuit with the input short-circuit containing the equivalent input noise voltage of Inv-Amp Inv e_A and its equivalent input noise current i_A , and the output noise voltage of e_{oTv} ; (b) Noiseless TIA circuit with the equivalent input noise voltage of the TIA e_T as the input signal, and the output noise voltage of e_{oTve} ; the equivalency of the above two circuits means $e_{oTv} = e_{oTve}$.

For the TIA, the circuit containing all noise sources with the input short-circuit is shown as Fig.s4-1(a), and the output noise is e_{oTv} . The noiseless circuit with the equivalent input noise voltage of the TIA e_T as the input signal is shown as Fig.s4-1(b), and the output noise is e_{oTve} . For calculating the equivalent input noise voltage of the TIA, the equations are established on the equivalency of the above two circuits, i.e. $e_{oTv} = e_{oTve}$. Therefore, by nodal analysis method,

$$E_T = E_A .$$

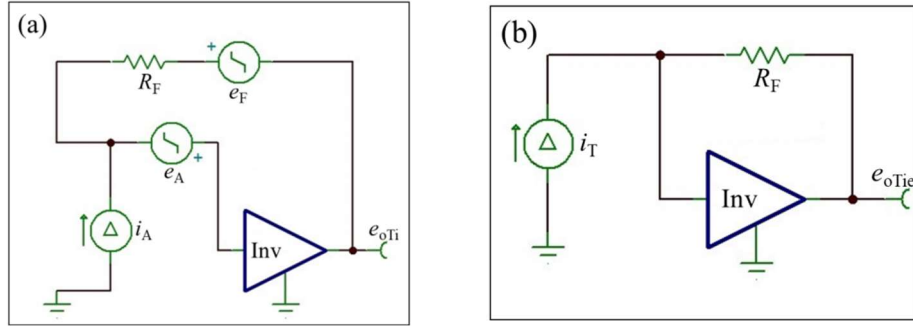


Figure s4-2 (a) TIA circuit with the input open-circuit containing the equivalent input noise current of Inv-Amp Inv e_A and its equivalent input noise current i_A , and the output noise current of e_{oTi} ; (b) Noiseless TIA circuit with the equivalent input noise current of the TIA i_T as the input signal, and the output noise voltage of e_{oTie} ; the equivalency of the above two circuits means $e_{oTi} = e_{oTie}$.

For the TIA, the circuit containing all noise sources with the input open-circuit is shown as Fig.s4-2(a), and the output noise is e_{oTi} . The noiseless circuit with the equivalent input noise current of the TIA i_T as the input signal is shown as Fig.s4-2(b), and the output noise is e_{oTie} . For calculating the equivalent input noise current of the TIA, the equations are established on the equivalency of the above two circuits, i.e. $e_{oTi} = e_{oTie}$. Therefore, by the nodal analysis method,

$$I_T = I_A + (E_A + E_F)/R_F .$$

Hence,

$$\begin{pmatrix} E_T \\ I_T \end{pmatrix} = \begin{pmatrix} 0 \\ 1/R_F \end{pmatrix} (E_F + E_A) + \begin{pmatrix} E_A \\ I_A \end{pmatrix} .$$

From $\begin{pmatrix} E_T E_T^* & E_T I_T^* \\ I_T E_T^* & I_T I_T^* \end{pmatrix}$, by Wiener-Khintchine theorem, $\begin{pmatrix} \overline{e_T^2} & \overline{e_T i_T^*} \\ \overline{i_T e_T^*} & \overline{i_T^2} \end{pmatrix}$ can be obtained. The two

matrix elements on the main diagonal are the equivalent input noise voltage PSD of the TIA $\overline{e_T^2}$ and its equivalent input noise current PSD $\overline{i_T^2}$. The two matrix elements on the sub-diagonal are its

equivalent input noise voltage-current PSD $\overline{e_T i_T^*}$ and equivalent input noise current-voltage PSD $\overline{i_T e_T^*}$.

$$\overline{e_T^2} = \overline{e_A^2} \quad , \quad (\text{s4.1})$$

$$\overline{i_T^2} = \overline{i_A^2} + 4k_B T / R_F + \overline{e_A^2} / R_F^2 \quad , \quad (\text{s4.2})$$

$$\overline{e_T i_T^*} = \left(\overline{i_T e_T^*} \right)^* \doteq \overline{e_A i_A^*} + \overline{e_A^2} / R_F \quad . \quad (\text{s4.3})$$

Here, the noise voltage PSD of R_F is $\overline{e_F^2} = 4k_B T R_F$.

The TIA is connected with the signal source circuit to form a STM-TIA. The equivalent input noise current PSD of a STM-TIA $\overline{i_{in}^2}$ can be obtained [S4R1-S4R3] by

$$\overline{i_{in}^2} = \overline{i_T^2} + \left(1/R_J^2 + (2\pi f)^2 C_U^2 \right) \overline{e_T^2} + (1/R_J + j2\pi f C_U) \overline{e_T i_T^*} + (1/R_J - j2\pi f C_U) \overline{i_T e_T^*} \quad . \quad (\text{s4.4})$$

Here, $C_U = C_I + C_J$. Putting Eq.(s4.1), (s4.2), and (s4.3) into Eq.(s4.4), $\overline{i_{in}^2}$ is

$$\begin{aligned} \overline{i_{in}^2} = & \overline{i_A^2} + 4k_B T / R_F + \overline{e_A^2} \left(1/R_J^2 + 1/R_F^2 + (2\pi f)^2 C_U^2 \right) \\ & + (1/R_J + j2\pi f C_U) \left(\overline{e_A i_A^*} + \overline{e_A^2} / R_F \right) + (1/R_J - j2\pi f C_U) \left(\overline{i_A e_A^*} + \overline{e_A^2} / R_F \right) \quad . \end{aligned} \quad (\text{s4.5})$$

S4.2 Noises of the proposed CryoSTM-TIA

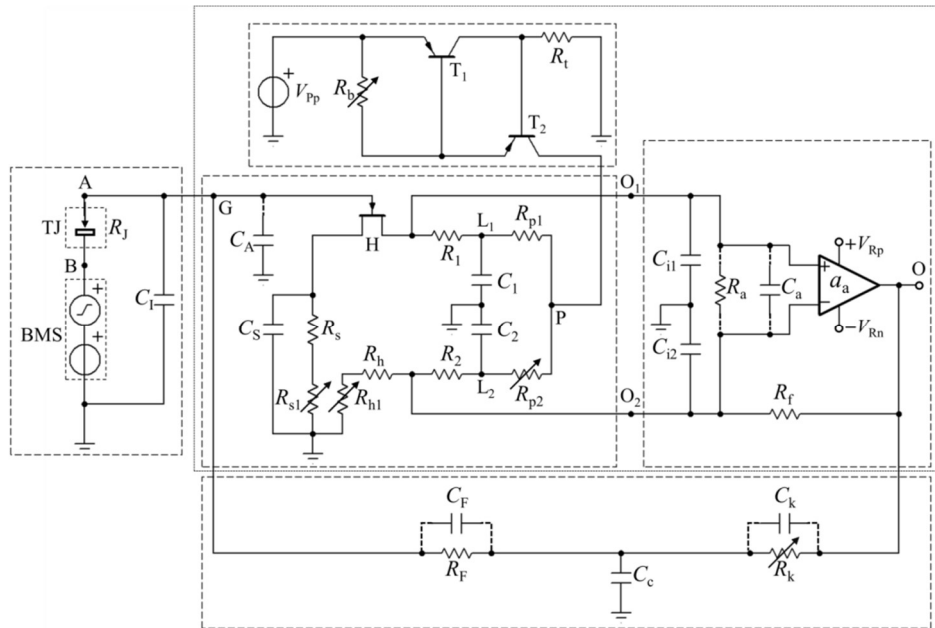


Figure s4-3 Circuit of the proposed CryoSTM-TIA. Inv-Amp of the proposed CryoSTM-TIA is shown in dotted box.

For the proposed CryoSTM-TIA shown as Fig.s4-3 (i.e. Fig.1 in Paper), its Inv-Amp is shown as Fig.s4-4. For the Inv-Amp, its $\overline{e_A^2}$, $\overline{i_A^2}$, $\overline{e_A i_A^*}$, and $\overline{i_A e_A^*}$ can be calculated by the nodal analysis method and Wiener-Khintchine theorem. Putting the results into Eq.(s4.5), the equivalent input noise current PSD of the proposed CryoSTM-TIA $\overline{i_{in}^2}$ is obtained.

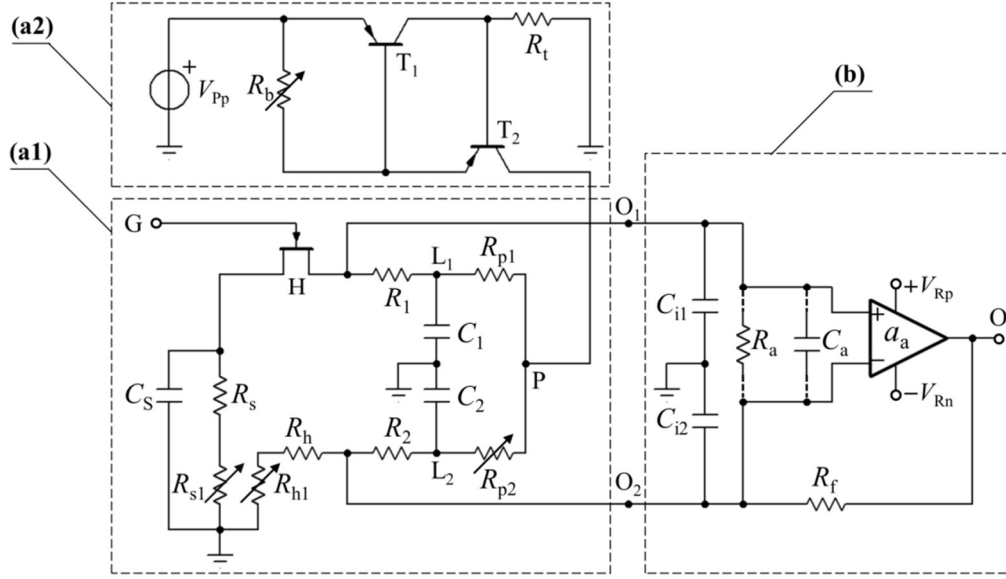


Figure s4-4 Inv-Amp circuit of the proposed CryoSTM-TIA. G is the input and O is the output. The single-transistor circuit in Pre-Amp is shown in dashed box (a1), the constant current source part in Pre-Amp is in dashed box (a2), and Post-amp is in dashed box (b).

S4.2.1 The equivalent input noise voltage and the equivalent input noise current of Inv-Amp

For the Inv-Amp, the equivalent input noise voltage and equivalent input noise current of transistor C-H are denoted as e_H and i_H respectively, and their harmonic components of f is are denoted as E_H and I_H respectively. g_m is the transconductance of C-H and g_d is channel conductance of C-H. The noise voltage of the resistors R_H is denoted as e_{RH} , and the harmonic components of f are denoted as E_{RH} . The noise voltage of the resistors R_1 , R_2 , and the feedback resistance R_f are denoted as e_{L1} , e_{L2} and e_f respectively, and the harmonic components of f are denoted as E_{L1} , E_{L2} , and E_f respectively. Here, $R_1 = R_2 = R_L$. All noises of R_H , R_1 , R_2 , and R_f above 1 kHz are thermal noise. $R_d = R_L / (1/g_d)$ and $R_{HL} = R_H / R_L$ are denoted. The equivalent input noise voltage and equivalent input noise current of Rear-OPA are denoted as e_a and i_a respectively, and the harmonic

components of f are denoted as E_a and I_a respectively. These noise sources are independent of each other. For the Inv-Amp consistent of the Pre-Amp and Post-Amp, its equivalent input noise voltage and equivalent input noise current as e_A and i_A , the corresponding harmonic components of f are E_A and I_A respectively.

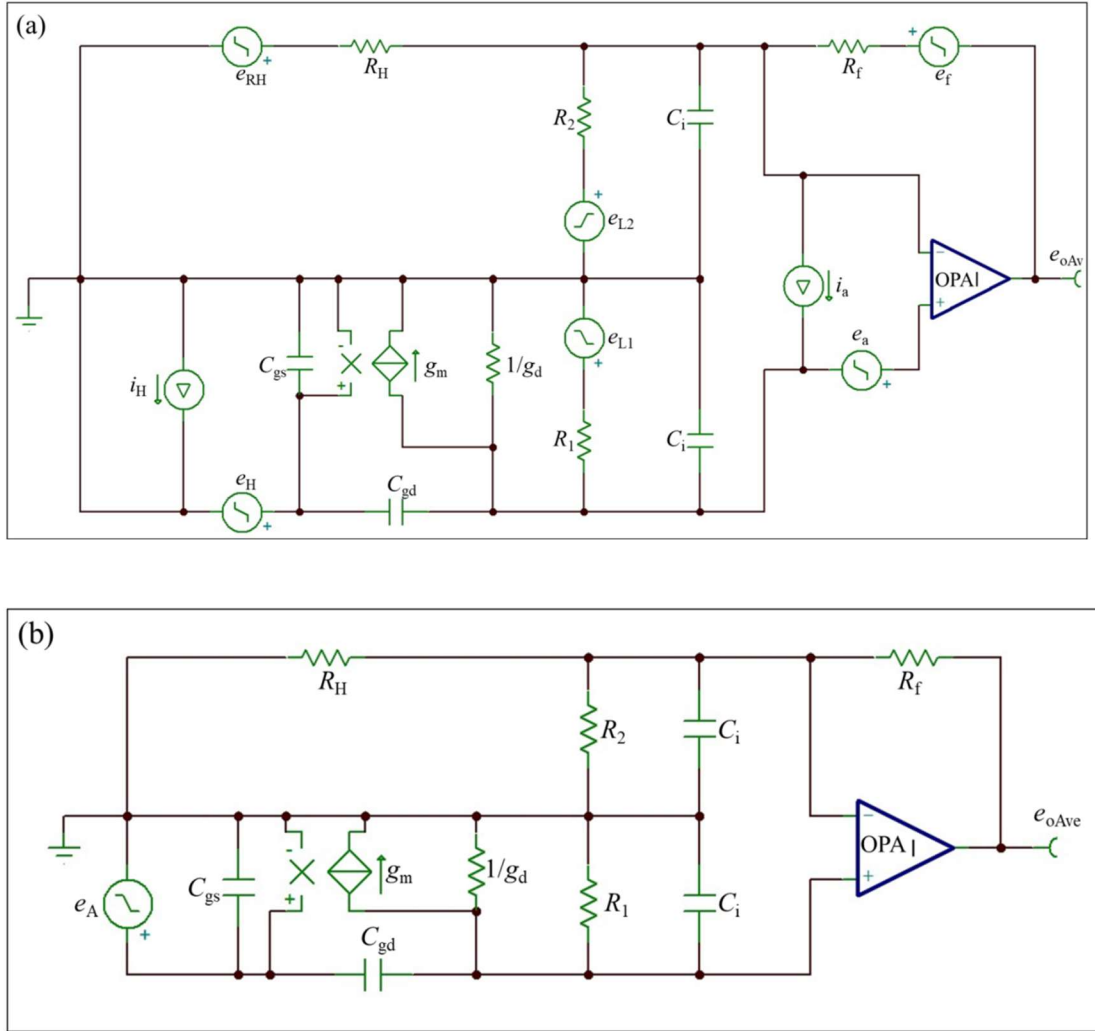


Figure s4-5 (a) Inv-Amp equivalent differential circuit with the input short-circuit containing all noise sources, and the output noise current of e_{oAv} ; (b) Noiseless Inv-Amp circuit with the equivalent input noise voltage of the Inv-Amp e_A as the input signal, and the output noise voltage of e_{oAve} ; the equivalency of the upper two circuits means $e_{oAv} = e_{oAve}$. In (a) and (b), the triangle OPA is the Rear-OPA.

The equivalent differential circuit of the Inv-Amp containing all noise sources with the input short-circuit is shown as Fig.s4-5(a), and the output noise is e_{oAv} . The noiseless circuit with the equivalent input noise voltage of the Inv-Amp e_A as the input signal is shown as Fig.s4-5(b), and the

are established on the equivalency of the upper two circuits, i.e. $e_{oAi} = e_{oAie}$. Therefore, by the nodal analysis method,

$$I_A \approx I_H + j(2\pi f)C_{Aj}E_{RH}Z_{HL}/(A_{vPj} R_H) - j(2\pi f)(C_{gs} + C_{gd})E_{L1}/(g_m R_L) + j(2\pi f)C_{Aj}E_{L2}Z_{HL}/(A_{vPj} R_L) \\ + j(2\pi f)C_{Aj}E_f Z_{HL}/(A_{vPj} R_f) - j(2\pi f)C_{Aj}E_a/A_{vPj} - j(2\pi f)[(C_{gs} + C_{gd})/g_m + C_{Aj}Z_{HL}/A_{vPj}]I_a, \quad (s4.7)$$

where, $C_{Aj} = C_{gs} + C_{gd}(1 + A_{vPj})$.

Thus,

$$\begin{pmatrix} E_A \\ I_A \end{pmatrix} = \begin{pmatrix} 0 \\ 1 \end{pmatrix} I_H + \begin{pmatrix} 1 \\ 0 \end{pmatrix} E_H + \begin{pmatrix} 1 \\ j(2\pi f)C_{Aj} \end{pmatrix} \frac{Z_{HL}E_{RH}}{A_{vPj}R_H} - \begin{pmatrix} 1 \\ j(2\pi f)(C_{gs} + C_{gd}) \end{pmatrix} \frac{E_{L1}}{g_m R_L} + \begin{pmatrix} 1 \\ j(2\pi f)C_{Aj} \end{pmatrix} \frac{Z_{HL}E_{L2}}{A_{vPj}R_L} \\ + \begin{pmatrix} 1 \\ j(2\pi f)C_{Aj} \end{pmatrix} \frac{Z_{HL}E_f}{A_{vPj}R_f} - \begin{pmatrix} 1 \\ j(2\pi f)C_{Aj} \end{pmatrix} \frac{E_a}{A_{vPj}} - \begin{pmatrix} 1/g_m + Z_{HL}/A_{vPj} \\ j(2\pi f)[(C_{gs} + C_{gd})/g_m + C_{Aj}Z_{HL}/A_{vPj}] \end{pmatrix} I_a. \quad (s4.8)$$

For the measured frequency of $f_m < 300$ kHz, $2\pi f C_i < 0.2$ mS with $C_i = 100$ pF, while $1/R_d = 1/R_L + g_d = 2$ mS and $1/R_{HL} = 1/R_L + 1/R_H = 6$ mS, so $A_{vPj} = g_m/[1/R_L + g_d + j(2\pi f)C_i]$ is approximately simplified to $-A_{vP} = g_m/(1/R_L + g_d) = g_m R_d$, Z_{HL} to $R_{HL}/(g_m R_d)$, and C_{Aj} to C_A . Ignoring the small quantities, such as the thermal noise of R_1 , R_2 , and R_f ,

$$\overline{e_A^2} \doteq \overline{e_H^2} + \left[(R_{HL}^2/R_H^2) \overline{e_{RH}^2} + \overline{e_a^2} \right] / A_{vP}^2 + (1 + R_{HL}/R_d) \overline{i_a^2} / g_m^2, \quad (s4.9)$$

$$\overline{i_A^2} \doteq \overline{i_H^2} + (2\pi f)^2 C_A^2 \frac{R_{HL}^2}{R_H^2} \frac{\overline{e_{RH}^2}}{A_{vP}^2} + (2\pi f)^2 C_A^2 \frac{\overline{e_a^2}}{A_{vP}^2} + (2\pi f)^2 \left[(C_{gs} + C_{gd}) + \frac{R_{HL}}{R_d} C_A \right]^2 \frac{\overline{i_a^2}}{g_m^2}, \quad (s4.10)$$

$$\overline{e_A i_A^*} = (\overline{i_A e_A^*})^* \doteq -j(2\pi f) \left[C_A \left(\frac{R_{HL}^2}{R_H^2} \frac{\overline{e_{RH}^2}}{A_{vP}^2} + \frac{\overline{e_a^2}}{A_{vP}^2} \right) + \left(C_{gs} + C_{gd} + \frac{R_{HL}}{R_d} C_A \right) \left(1 + \frac{R_{HL}}{R_d} \right) \frac{\overline{i_a^2}}{g_m^2} \right]. \quad (3.11)$$

Here, $\overline{e_H^2}$ is the equivalent input noise voltage PSD of the CNRS-HEMT C-H and $\overline{i_H^2}$ is their equivalent input noise current PSD. $\overline{e_a^2}$ is the equivalent input noise voltage PSD of the Rear-OPA and $\overline{i_a^2}$ is its equivalent input noise current PSD.

$\overline{e_a^2} = 2.25$ (nV)²/Hz and $\overline{i_a^2} = 4$ (pA)²/Hz in $f \geq 10$ kHz [S4R4]. In Eq.(s4.9)-(s4.11), $(R_{HL}^2/R_H^2) \overline{e_{RH}^2}$ is two orders of magnitude smaller than $\overline{e_a^2}$. $(1 + R_{HL}/R_d) \overline{i_a^2}/g_m^2$ is one order of magnitude smaller than $\overline{e_H^2}$ in Eq.(s4.9). $(C_{gs} + C_{gd} + C_A R_{HL}/R_d)^2 \overline{i_a^2}/g_m^2$ is one order of magnitude smaller than $C_A^2 \overline{e_a^2}/A_{vP}^2$ in Eq.(s4.10). $(C_{gs} + C_{gd} + C_A R_{HL}/R_d)(1 + R_{HL}/R_d) \overline{i_a^2}/g_m^2$ is

one order of magnitude smaller than $C_A \overline{e_a^2} / A_{vp}^2$ in Eq.(s4.11). Further ignoring the small quantities in Eq.(s4.9)-(s4.11),

$$\overline{e_A^2} \doteq \overline{e_H^2} + \overline{e_a^2} / A_{vp}^2, \quad (s4.12)$$

$$\overline{i_A^2} \doteq \overline{i_H^2} + (2\pi f)^2 C_A^2 \overline{e_a^2} / A_{vp}^2, \quad (s4.13)$$

$$\overline{e_A i_A^*} = \left(\overline{i_A e_A^*} \right)^* \doteq -j(2\pi f) C_A \overline{e_a^2} / A_{vp}^2. \quad (s4.14)$$

S4.2.2 The equivalent input noise current of the proposed CryoSTM-TIA

Putting Eq.(s4.12), (s4.13), and (s4.14) into Eq.(s4.5), the equivalent input noise current PSD of the proposed CryoSTM-TIA $\overline{i_{in}^2}$ is obtained as

$$\overline{i_{in}^2} = \overline{i_H^2} + 4k_B T / R_F + (1/R_J + 1/R_F)^2 \left(\overline{e_H^2} + \overline{e_a^2} / A_{vp}^2 \right) + (2\pi f)^2 \left(C_{IJ}^2 \overline{e_H^2} + C^2 \overline{e_a^2} / A_{vp}^2 \right), \quad (s4.15)$$

where $C_{IJ} = C_I + C_J$ and $C = C_A + C_I + C_J$. Eq.(s4.5) is Eq.(3.8) in Article.

[S4R1] A. van der Ziel, Noise in Solid State Devices and Circuits, Wiley-Inter-Science, New York, (1986).

[S4R2] Y.X. Liang, Low-noise large-bandwidth transimpedance amplifier for measuring scanning tunneling shot noise spectra in cryogenic STM and its applications, Ultramicroscopy, 234 (2022) 13466.

[S4R3] Z.H. Qian, Study on noise models algorithms and matrix descriptions for integrated circuits, J. Northeast Norm. Univ. 35 (2003) 41.

[S4R4] Data sheet of THS4021 OPA, <https://www.ti.com/lit/ds/symlink/ths4021.pdf>.3

Supplemental file 5: Estimating the DC tunneling current error for CryoSTM-TIA

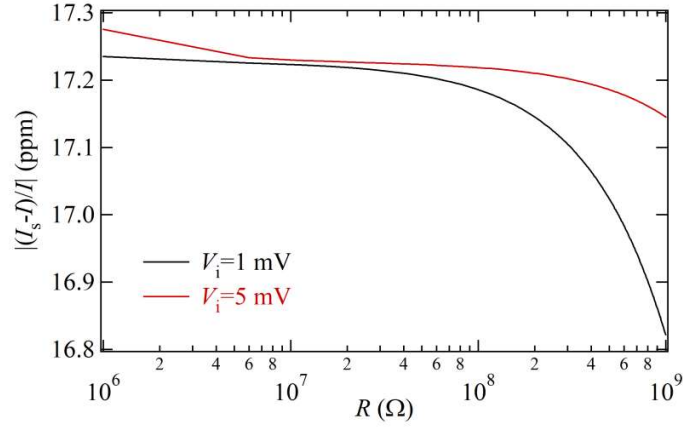


Figure s5-1 For the proposed CryoSTM-TIA, $Er = |I_s - I|/|I|$ vs. R ($R \in [1 \text{ M}\Omega, 1 \text{ G}\Omega]$) is simulated by TINA-TI with $V_i = 1$ mV (Black curve) and $V_i = 5$ mV (Red curve).

For the proposed CryoSTM-TIA, Fig. s5-1 shows the TINA-TI simulation results $Er = |I_s - I|/|I|$ vs. R ($R \in [1 \text{ M}\Omega, 1 \text{ G}\Omega]$) with $V_i = 1$ mV (Black curve) and $V_i = 5$ mV (Red curve). The simulation results show $Er < 20$ ppm, consistent with the calculated results in Article.

Supplemental file 6: Estimation of Inv-Amp input offset voltage

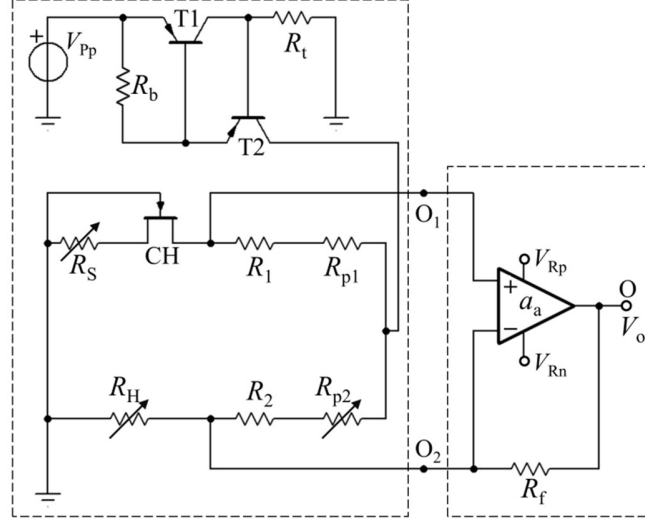


Figure s6-1 DC circuit of the inverting amplifier.

Table s6-1 Parameters of THS4021 as the Rear-OPA in Post-Amp

Open loop DC voltage gain a_{a0}	97.5 dB
Input offset voltage drift $ v_{\text{off}} /^{\circ}\text{C}$	15 $\mu\text{V}/^{\circ}\text{C}$
Input bias current $I_{\text{bp}}, I_{\text{bn}}$	3 μA
Input bias current drift $ i_{\text{bp}} /^{\circ}\text{C}, i_{\text{bn}} /^{\circ}\text{C}$	Estimated as 100 nA/ $^{\circ}\text{C}$
CMRR	95 dB
$a_c = a_{a0}/\text{CMRR}$	2.5 dB

The Pre-Amp in the left dashed box of Fig.s6-1 is made of CNRS-HEMT C-H. The source of C-H is grounded via a variable resistor R_S . The source of C-H is connected to R_1 . $R_1=R_2=1 \text{ k}\Omega$, $R_{L1}=R_1+R_{p1}$, $R_{p1}=10 \Omega$, $R_{L2}=R_2+R_{p2}$, and variable resistor R_{p2} can be adjustable from 0 to 20 Ω . $R_{L1} \approx R_{L2} \approx R_L=1 \text{ k}\Omega$. Its input (the gates of C-H) is grounded, and its two outputs O_1 and O_2 are suspended.

Adjust $R_{L1}=R_{L2}$. The current that the constant-current source supplies to the amplifier of the Pre-Amp is adjusted to $I_{\text{sour}}=2I_{\text{ds}}=2 \text{ mA}$. Adjust R_S and R_H , to let C-H at the ideal operating point ($I_{\text{ds}}, V_{\text{ds}})=(1 \text{ mA}, 100 \text{ mV})$, and the DC voltages at O_1 and O_2 are at the same value V_c . The gate-source voltage $V_{\text{gs}}=-I_{\text{ds}}R_S$, and $V_c=V_{\text{ds}}-V_{\text{gs}}$. I assume $V_{\text{gs}}=-100 \text{ mV}$ for the ideal operating point, so $R_S=100 \Omega$, $R_H=200 \Omega$, and $V_c=200 \text{ mV}$.

The Post-Amp is shown in the right dashed box of Fig.s6-1. Connecting the Pre-Amp to the Post-Amp, the inverting amplifier is formed. Adjust R_H and R_{p2} , to let C-H at the ideal operating point (I_{ds} , V_{ds}) = (1mA, 100mV), and the output DC voltage of inverting amplifier is 0.

For the inverting amplifier, the output voltage drift is v_o , the voltage drift at the output O_1 is v_1 , and it at O_1 is v_2 . The voltage drift at the output of the constant-current source is v_t , and the voltage drift at the source of C-H is v_s . By the following equations, the input offset voltage drift of the inverting amplifier can be obtained.

$$(v_t - v_1)/R_L + (v_t - v_2)/R_L = i_t, \quad (s6.7)$$

$$(v_t - v_1)/R_L = g_d(v_1 - v_s) - g_m v_s + i_{bp}, \quad (s6.8)$$

$$(v_o - v_2)/R_f + (v_t - v_2)/R_L = v_2/R_H + i_{bn}, \quad (s8.9)$$

$$v_s/R_s = g_d(v_1 - v_s) - g_m v_s, \quad (s6.10)$$

$$a_{a0}(v_1 + v_{off} - v_2) + a_c(v_1 + v_{off} + v_2)/2 = v_o, \quad (s6.11)$$

$$v_{OS} = v_o/a_{A0}. \quad (s6.12)$$

$$a_{A0} = -g_m R_f / (g_d R_H). \quad (s6.13)$$

where, v_{OS} is the input offset voltage drift of the Macro-OPA for 1 °C. The parameters of THS4012 are listed in Table s6-1. From the above six equations, v_{OS} , v_s , v_1 , and v_2 can be solved out as $v_{OS} \approx -i_t(1 + g_m R_s)/(2g_m) - v_{off}g_d/g_m$, $v_s \approx i_t R_s/2$, and $v_1 \approx v_2 \approx i_t(1 + g_m R_s)/(2g_d)$.

$i_t = -8 \mu A$ is the current drift of the constant-current source for 1 °C, and $|v_{off}| = 15 \mu V$ is the input offset voltage drift of the Rear-OPA for 1 °C. Hence, $|v_s| \approx 0.4 mV$, $|v_1| \approx 20 mV$, and $|v_{OS}|$ is about 0.5 mV. i.e., in Article, the drift of the gate-source voltage of C-H in the inverting amplifier is about 0.4 mV/°C, the drift of the drain-source voltage of C-H is about 20 mV/°C, and the input offset voltage drift of the inverting amplifier is about 0.5 mV/°C. When the temperature fluctuations of the bipolar junction transistors (BJTs) in the constant-current source are controlled within 0.0002 °C, the fluctuations at the drain of C-H is below 4 μV , and the fluctuation at the source of C-H is below 80 nV, so the operating point for C-H is little changed. The power of the constant-current source is about 24 mW. It is able to control the temperature fluctuations of the constant-current source within 0.0002 °C with the well-designed temperature Control System [S6R1].

[S6R1] W. Zhang, et al, Design of Precise Temperature Control System for Saturated Absorption Frequency Stabilization of DFB Laser, Semiconductor optoelectronics, 41(4) 560-565 (2020).